

A Survey of Air-to-Ground Propagation Channel Modeling for Unmanned Aerial Vehicles

Wahab Khawaja^{ID}, Ismail Guvenc^{ID}, David W. Matolak^{ID}, Uwe-Carsten Fiebig, and Nicolas Schneckenburger^{ID}

Abstract—In recent years, there has been a dramatic increase in the use of unmanned aerial vehicles (UAVs), particularly for small UAVs, due to their affordable prices, wide availability, and relative ease of operability. Existing and future applications of UAVs include remote surveillance and monitoring, relief operations, package delivery, and communication backhaul infrastructure. Additionally, UAVs are envisioned as an important component of 5G wireless technology and beyond. The unique application scenarios for UAVs necessitate accurate air-to-ground (AG) propagation channel models for designing and evaluating UAV communication links for control/non-payload as well as payload data transmissions. These AG propagation models have not been investigated in detail, relative to terrestrial propagation models. In this paper, a comprehensive survey is provided on available AG channel measurement campaigns, large and small scale fading channel models, their limitations, and future research directions for UAV communication scenarios.

Index Terms—Air-to-ground (AG), channel measurement, channel modeling, drone, large and small scale fading, sounding, unmanned aerial vehicle (UAV).

I. INTRODUCTION

UNMANNED aerial vehicles (UAVs), also commonly referred as “drones”, have long been used for military and specialized applications [1]–[5]. Owing to recent technological advancements, they have attracted major attention from industry for uses (“use cases”) from delivery to communications, surveillance, inspection, transportation, search and rescue, among others [6]–[15]. These UAVs can vary in size from small toys that fit in the palm of a human hand (where the “unmanned” designation obviously becomes unnecessary) to large military aircraft such as the General Atomics MQ-9 Reaper (commonly termed Predator) [16], with a wingspan over 15 m. The small battery powered toys can typically fly for up to 15 minutes, whereas the larger UAVs can be designed for long-endurance (30 hours) and high-altitude operations (higher than 15 km). According to Goldman Sachs, a

Manuscript received January 1, 2018; revised June 30, 2018 and December 24, 2018; accepted March 21, 2019. Date of publication May 8, 2019; date of current version August 20, 2019. This work was supported in part by NSF under Grant CNS-1453678, and in part by National Aeronautics and Space Administration (NASA) through Federal Award under Grant NNX17AJ94A. (Corresponding author: Wahab Khawaja.)

W. Khawaja and I. Guvenc are with the Department of Electrical and Computer Engineering, North Carolina State University, Raleigh, NC 27606 USA (e-mail: wkhawaj@ncsu.edu; iguvenc@ncsu.edu).

D. W. Matolak is with the Department of Electrical Engineering, University of South Carolina, Columbia, SC 29208 USA (e-mail: matolak@cec.sc.edu).

U.-C. Fiebig and N. Schneckenburger are with the German Aerospace Center (DLR), Institute of Communications and Navigation, 82234 Weßling, Germany (e-mail: uwe.fiebig@dlr.de; nicolas.schneckenburger@dlr.de).

Digital Object Identifier 10.1109/COMST.2019.2915069

\$100 billion market opportunity exists for UAVs in commercial, civil government, and military sectors combined between now and 2020 [17].

Wireless connectivity with UAVs is a major enabler for integration of UAVs into a national air space and for facilitating new use cases. However, UAV operating environments and scenarios introduce unique technical challenges, and these are recently being investigated by telecommunications companies such as AT&T [18], Vodafone [19], Ericsson [20], Nokia [21], [22] and Qualcomm [23], among others. One of the major challenges is to have realistic air-to-ground (AG) propagation models for various UAV operating environments and scenarios, in order to fulfill the ever increasing demands of high rate data transfer for emerging UAV applications. In particular, having accurate characterization of the AG channel is of paramount importance for designing robust and effective waveforms, modulation techniques, resource allocation and link adaptation approaches, and multiple antenna techniques.

The AG channel for UAVs has not been studied extensively when compared with the existing literature on the terrestrial propagation channels. The available AG propagation channel models used for higher altitude aeronautical communications generally cannot be employed directly for low-altitude UAV communications due to differences in channel scattering environment. Small UAVs may also possess distinct structural and flight characteristics such as different airframe shadowing features due to unique body shapes and materials, and potentially sharper pitch, roll, and yaw rates of change during flight. In this survey, we will provide a comprehensive, unified review of the existing work on UAV AG propagation channels. We will discuss recent channel measurement campaigns and modeling efforts to characterize the AG channel for UAVs. We will also describe future research challenges and possible enhancements relating to UAV propagation channels.

The rest of the paper is organized as follows. Section II provides a review of various use cases of interest for UAVs to provide some context, and gives a brief literature review on existing efforts for modeling propagation characteristics of aerial links. Subsequently, Section III explains some of the unique propagation channel characteristics for the UAV AG channels such as operating frequencies, scattering, antenna effects, and Doppler, and compares the differences with terrestrial channels. A review of some key considerations for AG channel measurements is provided in Section IV, including measurement frequencies, configurations, and environments, unique challenges for AG measurements, different sounding

waveform types for AG measurements, and the effect of elevation angle on measurement results.

Section V continues to review the existing UAV AG propagation measurements and some representative simulation studies in the literature. In particular, path loss and shadowing, delay dispersion, narrowband fading, Doppler spread, throughput and bit error rate characteristics, and the effects of different measurement environment types are reviewed for some existing studies in the literature. Section VI discusses AG propagation channel models, including models based on deterministic and stochastic models, their combination, and ray tracing simulations. After classification and review of different channel model types, we provide a survey of path loss and large scale fading models, airframe shadowing, small scale fading models, modeling of intermittent multipath components (MPCs), effect of frequency bands, and multiple-input-multiple-output (MIMO) propagation models. We also review the recent 3GPP AG UAV channel models, and provide a comparison of existing AG propagation models with each other and with traditional cellular and satellite channel models.

Future challenges and research directions for UAV channel measurements and modeling are provided in Section VII, and concluding remarks follow in Section VIII. All acronyms and variables used throughout this survey paper are given in Table I and Table II, respectively. Multiple tables and figures are provided to tabulate, classify, and review existing aerial channel modeling studies in the literature in a unified manner. Table III provides a review of AG channel measurements in the literature along with their measurement configurations, Table IV classifies related measurement studies with respect to five different measurement environments, Fig. 2 provides a taxonomy of measurement scenarios and related literature in terms of aerial vehicle type and measurement environment, Table V reviews the existing literature on large scale AG propagation and summarizes key path loss parameters, Fig. 5 classifies the literature on UAV AG channel models in terms of deterministic and stochastic models, and finally Table VI summarizes small scale AG model parameters documented in the literature.

II. UAV USE CASES AND LITERATURE REVIEW

Various organizations have developed classifications for UAVs according to size, with designations large, medium, and small being typical. In the U.S., the Federal Aviation Administration (FAA) has issued rules for small UAVs weighing less than 55 pounds (25 kg) [24]. Highlights of these rules include the requirement for a visual line-of-sight (LOS) from pilot to aircraft, flight under daylight or during twilight (within 30 minutes of official sunrise/sunset) with appropriate lighting for collision avoidance, a maximum flight ceiling of 400 feet (122 m) above the ground (higher if the UAV is within 122 m of a construction site), and a maximum speed of 100 mph (87 knots, or 161 km/h). Restrictions also apply regarding proximity to airports, and generally, a licensed pilot must operate or supervise UAV operation. In this survey paper our focus is on the smaller UAVs, and specifically on the air-ground (AG) channel between these UAVs and the GSs with

which they communicate. These GSs are also usually the UAV control stations.

A. UAV Use Cases

Use of commercial UAVs has recently seen exceptional growth that is forecast to continue in the foreseeable future. The easy operability, availability of multiple flight controls, high maneuverability, and increasing payload weight have led to the use of UAVs for many real time civilian applications. This includes for examples remote surveillance, filming, disaster relief, transport of goods, and communication relaying, as well as recreation. According to statistics provided by the market research company Tractica, the shipment of commercial UAV units is expected to reach 2.7 million in 2025 with the services offered rising to \$8.7 billion in the next decade [25].

Another promising application of UAVs is in supporting broadband cellular communications, and wireless local area networks (WLANS) such as IEEE 802.11. Cellular use may be in hot spot areas during peak demand events, and in cases of a natural calamity where the existing communication infrastructure is damaged. It is expected that future 5G implementation will include UAVs as autonomous communicating nodes, possibly for providing low latency and highly reliable communications. Qualcomm is testing the operability of UAVs for current LTE and future 5G cellular applications [26]. Facebook and Google are also exploring the possibility of using UAVs for Internet connectivity to remote areas [27].

B. Literature Review on Aerial Propagation

The available UAV based AG wireless propagation channel research can be largely categorized into two major portions. The first one is payload communications, where the payload can be narrow-band or wide-band and is mostly application dependent. The second one is control and non-payload communications (CNPC) for telemetric control of UAVs. Most of the CNPC employs the unlicensed bands, e.g., 2.4 GHz, and 5.8 GHz; this is not preferred by the aviation community as these bands can be congested and may be easily jammed. In the USA, CNPC is potentially planned for a portion of L-band (0.9 GHz - 1.2 GHz) and C-band (5.03 GHz - 5.091 GHz), although as is common in spectrum allocation, use of these bands is still being negotiated [28], [29]. Channel measurements and modeling for UAVs are (other than bandwidth and carrier frequency) largely independent of whether signaling is for payload or CNPC.

AG communications can be traced back to 1920 [30], with manually operated radio telegraphs. Lower frequency bands were used in the early 1930s but did not support simultaneous voice communications in both directions (AG and ground-to-air (GA)). From the early 1940s, double sideband amplitude modulation (DSB-AM) in the very high frequency (VHF) band (118 MHz - 137 MHz) was adopted for voice communications between pilots and ground controllers. This system supported a maximum of 140 channels until 1979. Multiplexing and multiple access were frequency division with *manual* channel assignment by air traffic control. In more dense air traffic

spaces, to enable larger numbers of simultaneous transmissions, 25 kHz DSB-AM channels were subdivided into three channels of width 8.33 kHz.

The civilian aeronautical AG communications continues to use the reliable analog DSB-AM system today, although since 1990 some small segments of the VHF band in some geographic locations are being upgraded to a digital VHF data link that can in principle support 2280 channels [31], [32]. This system employs time-division as well as frequency-division, with single-carrier phase-shift keying modulation. Military AG communications uses different frequency bands (ultra-high frequency) and modulation schemes for short and long ranges [33]. Due to very low data rates, the civil aviation systems cannot support modern AG communication requirements. In 2007, use of portion of the L-band was suggested for new civil aviation systems, and two such systems known as L-band Digital Aeronautical Communications Systems, or LDACS, were developed [32]. Due to compatibility with numerous existing systems that operate in the L-band, the LDACS system is still being refined. LDACS is currently being standardized by the International Civil Aviation Organization.

There are numerous studies available in the literature on the characteristics of aeronautical channels [31], [34]–[37]. Aeronautical communications can be broadly classified into communications between the pilot or crew with the ground controller and wireless data communication for passengers. Both of these types of communication are dependent on the flight route characteristics. In [34] the propagation channel is divided into three main phases of flight, termed as parking and taxiing, en-route, and take off and landing. Each phase of flight was described by different channel characteristics (type of fading, Doppler spread, and delay), but this relatively early paper was not comprehensive nor fully supported by measurements.

There are also long distance AG propagation channel studies available for satellites and high altitude platforms (HAPs). The AG propagation channel in these studies can be considered as a UAV communication channel, but due to long distances from the earth surface, normally greater than 17 km, modeling of these links may also need to take into account upper atmospheric effects. Depending on frequency and UAV altitude, they may also be much more susceptible to lower tropospheric effects such as fading from hydrometeors [38]. For most of these longer distance platforms, a LOS component is required because of power limitations, hence the AG channel amplitude fading is typically modeled as Ricean [39]. As the deployment of UAVs as communication nodes in the near future is expected to be at much lower altitudes compared to that of HAPs and satellites, in this survey we focus only on lower altitude UAV AG propagation channels.

C. Existing Surveys on UAV AG Channel Propagation

There are some survey studies available for UAV AG propagation channel measurements and modeling [37], [40], [41]. In [37], a survey on wideband AG propagation channel was provided with focus on the L-band and C-band envisioned as possible candidates for future non-payload AG communications. A tapped delay line model for time varying

channel was provided. A general finding was that no accurate and comprehensive wideband AG propagation channel model based on empirical data existed for L-band and C-band. However, the literature review content in the survey is now dated and new research has since appeared in the literature. A similar short description of overall propagation channel characteristics for UAVs was provided in [40] with analysis of two ray geometrical model and its applications in different scenarios. Limitations of existing AG channel models for UAVs were also discussed.

A recent survey on AG propagation channel modeling was provided in [41]. The survey discussed measurement and analytical channel models available in the literature. The AG propagation channel measurements were divided into three parts. The first part covered narrowband, and wideband channel measurements, the second part discussed channel measurements using 802.11 radios, whereas the third part covered the cellular infrastructure based AG propagation channel measurements. A table of AG propagation channel measurements available in the literature was also provided. Additionally, large scale and small scale fading statistics and their respective models available in the literature were provided. The survey also covered analytical channel models from the literature on AG propagation. The analytical channel models were divided into three categories, namely, deterministic, stochastic (based on time delay line (TDL)), and geometric. Additionally, the survey provided air-to-air (AA) channel characterization studies from the literature with a common result of small path loss exponent (PLE) as compared to terrestrial or AG propagation. Towards the end of the survey, important issues relating to AG propagation were discussed including airframe shadowing, stationary interval and diversity gain.

III. UAV AG PROPAGATION CHANNEL CHARACTERISTICS

In this section, salient characteristics of UAV AG propagation channel are described. A common AG propagation scenario is shown in Fig. 1 in the presence of terrestrial obstacles which are also commonly referred as *scatterers*. In the figure, h_G , h_S , h_U represents the height of the ground station (GS), scatterers, and UAV above the ground, respectively, d is the slant range between the UAV antennas and the GS, and θ is the elevation angle between GS and UAV antennas. (We note that airborne scatterers may be present as well, but for this paper, for the AG link, we neglect this secondary condition.)

A. Comparison of UAV AG and Terrestrial Propagation

The AG channel exhibits distinctly different characteristics from those of other well studied terrestrial communication channels, e.g., the urban channel. There is the inherent advantage over terrestrial communications in terms of a higher likelihood of LOS propagation. This reduces transmit power requirements and can translate to higher link reliability as well. In cases where only non-LOS (NLOS) paths exist, when the elevation angle to the UAV is large enough, the AG channel may incur smaller diffraction and shadowing losses than near ground terrestrial links.

On the other hand, the AG channel can exhibit significantly higher rates of change than typical terrestrial communication

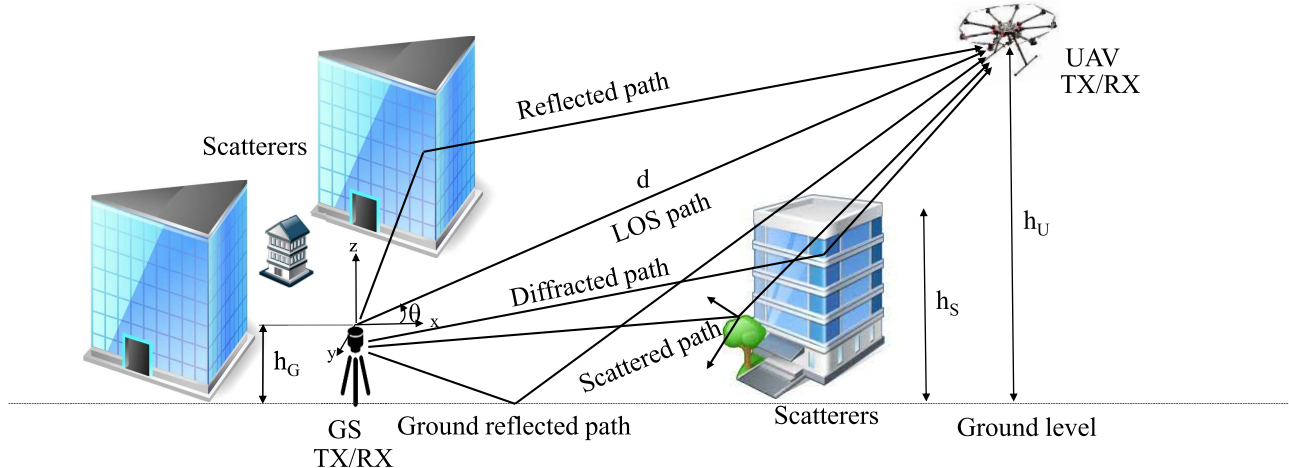


Fig. 1. A typical air-to-ground propagation scenario with a UAV.

channels because of UAV velocities. When the channel is modeled statistically, this can mean that the channel's statistics are approximately constant (the channel is wide-sense stationary (WSS)) for only a small spatial extent. This is often loosely termed "non-stationarity." If the UAV is not in the direct vicinity of scattering objects or the GS, the characteristics of the channel could instead actually change very slowly, especially for hovering UAVs. In such a case, adverse propagation conditions, e.g., deep fades of the received signal, may last several seconds or even minutes, hence common communication techniques of interleaving or averaging would not be effective. In many cases, when UAV altitudes are well above scattering objects, the AG channel's "non-stationarity" will be attributable to the direct surroundings of the GS, e.g., the close by buildings or the ground surface composition around the GS.

Additionally, AG communications with UAVs face many other challenges, due to arbitrary mobility patterns and diverse types of communication applications [42]–[45]. As an aerial node, some of the UAV specifics that need to be taken into account include airframe shadowing, mechanical and electronic noise from UAV electronics and motors, and finally antenna characteristics, including size, orientation, polarization, and array operation (e.g., beam steering) for MIMO systems. For UAVs in motion, the effect of Doppler shifts and spread must also be considered for specific communication applications [46], [47]. For a given setting, an optimum UAV height may need to be considered, e.g., for maintaining LOS in that environment [48].

B. Frequency Bands for UAV AG Propagation

As with all communication channels, a fundamental consideration is the frequency band, since propagation characteristics can vary significantly with frequency. There are typically two popular bands, 2.4 GHz and 5.8 GHz, used by commercial UAVs for CNPC operations during flight. However, other frequency bands may be used for additional features, e.g., for transferring videos from the UAV to the GS at 3.4 GHz. The 5.8 GHz band is a better choice than the 2.4 GHz for majority of scenarios, because of lower interference. For the L and

C-bands envisioned for CNPC, and for the currently popular unlicensed bands for payload communications, tropospheric attenuations from atmospheric gases and hydrometeors are mostly negligible. This will not be true for operation at higher frequency bands, e.g., at Ku, Ka, and other so-called millimeter wave (mmWave) bands, which may be as high as 100 GHz. These higher frequency bands can hence suffer both larger free-space path loss (FSPL) as well as tropospheric attenuations. Because of this, these frequency bands will generally be used for short-range AG links.

In contrast to the attenuation characteristics compared with lower frequency bands, mmWave bands offer a large amount of bandwidth, which is their primary appeal for 5G cellular systems. Large bandwidths can be more robust to the larger values of Doppler shift and Doppler spread encountered with UAVs moving at high velocity. The mmWave bands may be supported by UAVs in the future for high speed data applications as communication payload; however, for CNPC, mmWave bands may not be a good option due to higher attenuation and smaller diffractions, making these bands unreliable in case of even small blockages.

C. Scattering Characteristics for UAV AG Propagation

In an AG propagation channel using UAVs, the MPCs appear due to reflections from the earth surface, from terrestrial objects (ground scatterers), and sometimes from the airframe of the UAV itself. The characteristics of the channel will be dependent on the material, shape, and size of the scattering objects. The strongest MPC apart from the LOS component in an AG propagation scenario is often the single reflection from the earth surface. This gives rise to the well known two ray model.

For high enough frequencies, the scatterers on the ground and around the UAV can be modeled as points scatterers on the surface of two respective cylinders or spheres [49], [50] or ellipsoids, and these can be bounded (truncated) by intersection of the elliptical planes on the ground [51], [52]. These topologies can help in deriving geometrical characteristics of the AG propagation scenario. The distribution of

TABLE I
ACRONYMS USED IN THIS PAPER

Acronym	Text	Acronym	Text
AA	Air-to-air	AG	Air-to-ground
AWGN	Additive white Gaussian noise	BER	Bit error rate
BPSK	Binary phase shift keying	BW	Bandwidth
CDF	Cumulative distribution function	CFO	Carrier frequency offset
CIR	Channel impulse response	CNPC	Control and non-payload communications
CSI	Channel state information	CTF	Channel transfer function
CW	Continuous wave	DPP	Doppler power profile
DS	Doppler spread	DSB-AM	Double sideband amplitude modulation
DS-SS	Direct sequence spread spectrum	FAA	Federal aviation administration
FCC	Federal Communications Commission		
FBMC	Filter bank multicarrier	FMCW	Frequency modulated continuous wave
Freq.	Frequency	FSPL	Free-space path loss
GA	Ground-to-air	GMSK	Gaussian Minimum Shift Keying
GPS	Global positioning system	GS	Ground station
GSM	Global system for mobile communication	HAP	High altitude platform
ICI	Inter-carrier interference	Infs.	Infrastructure
IS-GBSCM	Irregular shaped geometric based stochastic channel model	LAP	Lower altitude platform
LDACS	L-band digital aeronautical communications	LOS	Line-of-sight
LTE	Long term evolution	MIMO	Multiple-input-multiple-output
MISO	Multiple-input-single-output	Mod. Sig.	Modulated signal
MPC	Multipath component	MSK	Minimum shift keying
NGSCM	Non-geometric channel model	NLOS	Non-line-of-sight
OFDM	Orthogonal frequency-division multiplexing	OLOS	Obstructed line-of-sight
PAPR	Peak to average power ratio	PDP	Power delay profile
PG	Path gain	PL	Path loss
PLE	Path loss exponent	PRN	Pseudo-random number
PSD	Power spectral density	RF	Radio frequency
RMS-DS	Root mean square-delay spread	RS-GBSCM	Regular shaped geometric based stochastic channel model
RSS	Received signal strength	RSSI	Received signal strength indicator
RSRQ	Reference signal receive quality	RTT	Round trip time
RX	Receiver	Satel.	Satellite
SDMA	Space-division multiple access	SIMO	Single-input-multiple-output
SISO	Single-input-single-output	SNR	Signal-to-noise-ratio
TDL	Tap-delay-line	TDMA	Time division multiple access
Terres.	Terrestrial	TOA	Time-of-arrival
TX	Transmitter	UAS	Unmanned aerial systems
UAV	Unmanned aerial vehicle	UMTS	Universal Mobile Telecommunications Service
UWB	Ultra-wideband	Vehic.	Vehicular
VHF	Very high frequency	WSS	Wide-sense stationary
3GPP	3rd Generation Partnership Project		

scattering objects, on land or water, can be modeled stochastically, and this concept can be used to create so-called geometrically-based stochastic channel models (GBSCMs). For aircraft moving through an area above such a distribution, this gives rise to intermittent MPCs [53], as also seen in vehicle-to-vehicle channels.

In case of propagation over water the path loss (PL) is similar to that of free space [54], with a strong surface reflection. The other MPCs from the water surface are weaker, and of approximately equal power and time-of-arrival (TOA), whereas MPCs from obstacles on the water surface, e.g., large ships, can be stronger.

D. Antenna Configurations for UAV AG Propagation

The antenna is one of the critical components for AG communications due to limited space, and limitations of the aerodynamic structure [55], [56]. Factors that affect AG link performance are the number, type and orientation of the antennas used, as well as the UAV shape and material properties.

The majority of AG channel measurements employ stand alone (single) antennas, whereas in [57], an antenna array is used. There are some single-input-multiple-output (SIMO) and MIMO antenna configurations available in the literature for AG propagation measurements [58], [59]. Omni-directional antennas are most popular for vehicular communications due to their superior performance during motion, whereas directional antennas (having better range via directional gain) can perform poorly during motion due to mis-alignment losses. With high maneuverability of UAVs during flight, omnidirectional antennas are generally better suited than directional antennas. A potential major drawback of any antenna on-board UAVs is the shadowing from the body of the UAV. Similarly, orientation of antennas on-board UAVs can affect the communication performance [60], [61]. The omni-directional antenna orientation is found to affect the received signal strength (RSS) and the system throughput. A better throughput performance was reported with horizontal-horizontal orientation as compared to vertical-vertical orientation in [60], whereas in [61], it was observed that horizontal antenna orientation can

TABLE II
VARIABLES USED IN THIS PAPER

Acronym	Text
A_m	Median attenuation as compared to FSPL
a	Amplitude of the MPC
b	Correction factor
c	Speed of light
d	Link distance between TX and RX
d_h	Horizontal distance between UAV and base station
d_0	Reference distance between TX and RX
f	Frequency instance
f_c	Carrier frequency
f_d	Doppler frequency shift of the MPC
f_{MHz}	Frequency in MHz
Δh	Height difference between UAV and GS
h_G	Ground station height
h_{RX}	Height of receiver
h_S	Height of scatterer
h_{TX}	Height of transmitter
h_U	UAV altitude above ground
G_A	Gain from the environment
G_{Gr}	Antenna gain for the ground reflected component
G_{LOS}	Antenna gain for LOS component
K -factor	Ricean K -factor
L_{rts}	Loss due to roof top to street diffraction and scattering
L_{msd}	Loss due to multi-screen diffraction
M	Total number of MPCs
n	Frequency dependent factor
p	MPC persistence coefficient
P_{d_0}	Received power at d_0
P_R	Received power
P_T	Transmit power
PL	Modified FSPL
PL_0	Reference path loss
PL_b	Base propagation loss
PL_{CI}	Close in PL
PL_{DS}	Dual slope PL
PL_F	FSPL
PL_{FI}	Floating intercept PL
PL_{LOS}	PL for LOS
PL_m	Median propagation loss
PL_{NLOS}	PL for NLOS
r	Horizontal distance between UAV and GS
r_1	LOS component path length
r_2	Ground reflected component path length
t	Time instance
v	Velocity of UAV
v_{\max}	Maximum speed
X	Shadowing random variable
X_{FS}	Random variations in the CI PL model
X_{FI}	Random variations in the FI PL model
X_{DS}	Random variations in the DS PL model
γ_s	Propagation loss slope
Γ	Ground reflection coefficient
α_0	Adjustment factor
α	Slope of linear least square regression fit
β	Y-intercept point for the linear least square regression fit
Θ	Aggregated phase angles
θ	Elevation angle
θ_{Gz}	Grazing angle
ϕ	Phase of the MPC
$\Delta\psi$	Phase difference between the LOS and ground reflected MPC
γ	Path loss exponent
τ	Delay of the MPC
λ	Wavelength of the radio wave
σ	Standard deviation of shadow fading
ς	Ratio of built up area to total area
ξ	Mean number of buildings per unit area
Ω	Height distribution of buildings

help to overcome the difference in the yaw, similarly, vertical orientation was found to perform better during tilting of UAV.

The use of multiple antennas to enable diversity can yield spatial diversity gains even in sparse multipath environments [62], [63]. It was demonstrated that using measurements that employ MIMO and SIMO in AG propagations can yield spatial diversity dependent on the antenna geometry and surrounding environment. Similarly, multiple antennas can be used for spatial selectivity such as beam forming/steering. However, due to limited space on-board UAVs, space diversity using multiple antennas is difficult to achieve, especially for lower carrier frequencies. Beamforming using antenna arrays operating at mmWave frequencies, for example, can be used to overcome fading and improve coverage, but array processing will require high computational resources on-board. The employment of MIMO systems for enhancing the channel capacity of the AG propagation channel has been suggested in [64], [65]. By changing the diameter of a circular antenna array and the UAV flying altitude, different values of MIMO channel capacity were obtained [64]. On the other hand, in [65], optimizing the distance between the antenna elements using linear adaptive antenna arrays was proposed to increase MIMO channel capacity.

E. Doppler Effects

Doppler shifts can introduce carrier frequency offset (CFO) and inter-carrier interference (ICI), especially for orthogonal frequency division multiplexing (OFDM) implementations. There are several studies that consider modeling of Doppler spread [34], [46], [47], [66]–[70] for AG scenarios. Some channel access algorithms, e.g., multi carrier code division multiple access, have been shown to be robust against Doppler spread in AG propagation [71], while Doppler spread is controlled by adjusting the carrier spacing of OFDM.

Due to UAV motion, there are Doppler frequency shifts that depend on the velocity of the UAV and the geometry. Higher Doppler frequency presents a problem if the different signal paths are associated with largely different Doppler frequencies, yielding large Doppler spread. This can happen if the aircraft is relatively close to the GS. If the aircraft is further away from the GS, and at sufficient altitude, the paths should all have a very similar Doppler frequency as the objects in the close surroundings of the GS causing MPCs are seen all under similar angles from the aircraft. The effect of a large Doppler frequency that is constant for all MPCs should be well mitigated by frequency synchronization.

In order to describe the statistical characteristics of a fading channel, typically first and second order fading statistics are used. The majority of the AG propagation literature discusses first order fading statistics. The second order statistics of envelope level crossing rate and average fade duration are discussed in [49], [68], but many authors address other second order properties, primarily correlation functions in the time or frequency domains.

IV. AG CHANNEL MEASUREMENTS: CONFIGURATIONS, CHALLENGES, SCENARIOS, WAVEFORMS

Several AG channel measurement campaigns using piloted aircraft and UAVs have been recently reported in the literature. These measurements were conducted in different

environments and with different measurement parameters. In this section, we provide a brief classification of these measurements based on environmental scenario, sounding signal, carrier frequency, bandwidth, and antenna specifications and placement. As available, we also provide UAV type and speed, heights of UAV and GS from terrain surface, link distance between transmitter (TX) and receiver (RX), elevation angle, and the channel statistics provided by the cited authors. These channel measurement parameters are given in Table III.

In the reported AG propagation measurements, either TX or RX on UAV/GS is stationary. Measurements with both TX and RX moving for AG propagation are rare. A notable contribution of wide-band AG propagation measurements is available in the form of multiple campaigns conducted in the L and C bands using SIMO antenna configuration for different terrain types and over water/sea [53], [54], [58], [73]–[79]. The rest of the cited channel measurements are conducted in different frequency bands ranging from narrow-band to ultra-wideband (UWB) with various types of sounding signals.

A. Channel Measurement Configurations

These channel measurements used different types and configurations of antennas. The most commonly used antenna type is omni-directional and the most commonly used configuration is single-input-single-output (SISO). The positioning of an antenna on the UAV is important to avoid both shadowing from the airframe and disruption of the aircraft's aerodynamics. In the majority of measurements the antennas were mounted on the bottom of the aircraft's fuselage or wings. The orientation of antennas on UAV and ground can also affect the signal characteristics [60], [61], [84], [85]. This characteristic is most important during banking turns, and when the aircraft pitch angle deviates from horizontal. The elevation angle between the TX and the RX antennas is dependent on the height of UAV and GS and often continuously varies during the flight.

In the majority of the communication applications envisioned for UAVs, the aerial node is expected to be stationary (or mostly so) in space for a given time. As noted, for communications with a mobile UAV, the velocity will affect the channel statistics. For UAVs operating at higher velocities, the coherence time of the channel decreases, and this translates into a larger Doppler spread. For connections to multiple UAVs, where hand-overs are required, this means that the number of handovers will also generally increase with velocity, and this will require additional processing. Additionally, higher velocities will result in increased air friction and mechanical turbulence that generally result in increased noise levels. Many of the AG channel measurements in the literature have been conducted with fixed wing aircraft with maximum speeds varying from 17 m/s to 293 m/s. The speed of rotorcraft and air balloons is much less than that of fixed wing aircraft, and ranges from 8 m/s to 20 m/s.

The height of the UAV above ground is an important channel parameter and will also affect the channel characteristics. For example, increasing the height of the UAV usually results in reduced effect of MPCs [93] from surrounding scatterers. Another benefit of higher UAV altitude is larger coverage area on the ground. Similarly, the height of GS will also affect the

channel characteristics. For a given environmental scenario, there may be an optimal height of the GS [72], e.g., this might be a balancing of attenuation and multipath diversity.

Example propagation measurements using rotorcraft and air balloons during flight and hovering are available in [61], [68], [72], [85]. These AG propagation measurements were obtained at different UAV heights ranging from 16 m to 11 km, and link distances 16.5 m to 142 km. The UAV latitude, longitude, yaw, pitch, and roll readings are typically obtained from global positioning system (GPS) RXs and often stored on-board.

Apart from conventional AG channel sounding, there are some indirect UAV AG channel measurements available from use of radios employing different versions of protocols of the IEEE 802.11 standards [60], [61], [84], [85]. The IEEE 802.11 supported devices offer a very flexible platform and may provide insight for UAV deployments in different topologies and applications, e.g., UAV swarms. Yet because of the specific features of 802.11, the resulting measurements are applicable to particular protocol setup and radio configuration, and rarely provide detailed propagation channel characteristics.

AA communications with UAVs has not been studied extensively in the literature [94]. The AA communications is particularly important for scenarios where multiple drones communicate among a swarm. This swarm then usually communicates with one or more GS via a back-haul link from one or several of the UAVs. The AA communications is similar to free space with a strong LOS and often a weak ground reflection, but this is dependent on the flight altitude and environment. The communication channel is mostly non-dispersive for higher altitudes but can be rapidly time-varying, dependent on the relative velocities of the UAVs and the scattering environment [95].

B. Challenges in AG Channel Measurements

There are many challenges in AG channel measurement campaigns as compared to terrestrial measurements. The biggest challenges are the payload limitation of the UAVs, and the operating range and height of UAVs, which in the USA is set by the FAA [96]. Larger UAVs also incur larger test costs. Due to restrictions on the height of UAVs above ground, UAVs at lower altitudes have lower LOS probability and are hence more susceptible to shadowing, especially in suburban and urban areas. Due to limitations on payload, higher transmit power measurements on-board the UAVs are difficult to achieve, and similarly, complex RX processing on-board UAVs can consume a prohibitive amount of power.

Other challenges include wireless precise frequency synchronization for channel measurements, varying conditions of the terrain during flight, meteorological conditions (winds and rain), antenna positioning on the UAV, precise location measurement of UAVs in space over time, diverse telemetry control for different types of UAVs having specific latencies, bandwidth and reliability issues, and limited flight time for most small UAVs due to limited battery life [42]–[44]. Due to the motion of UAVs in three dimensional space, it is challenging to precisely measure the distance between the UAV and the GS. Momentary wind gusts that cause sudden shifts in UAV position can make it difficult to accurately track the UAV path.

TABLE III
REVIEW OF IMPORTANT EMPIRICAL AG CHANNEL MEASUREMENT STUDIES IN THE LITERATURE AND THEIR MEASUREMENT CONFIGURATIONS ON SOUNDING WAVEFORM, FREQUENCY, BANDWIDTH, TRANSMIT POWER, UAV TYPE, TRANSMIT/RECEIVE HEIGHT

Ref.	Scenario	Sound. Sig.	Freq. (GHz)	BW (MHz)	Antenna and mounting	P_T (dBm)	UAV, v_{max} (m/s)	h_U, h_G , d (m)	θ (deg.)	Channel statistics
[68]	Urban	CW	2	.0125	1 Monopole on UAV for TX, 4 on GS for RX	27	Air balloon, 8	170, 1.5, 6000	1-6	P_R , Auto-correlation of direct and diffuse components
[72]	Open field, suburban	PRN	3.1 - 5.3	2200	1 Dipole on UAV for TX and 1 on GS for RX	-14.5	Quad-copter, 20	16, 1.5, 16.5	-	PL, PDP, RMS-DS, TOA of MPCs, PSD of sub-bands
[53], [54], [58], [73]-[79]	Urban, suburban, hilly, desert, fresh water, harbor, sea	DS-SS	0.968, 5.06	5, 50	1 directional antenna on GS for TX, 4 monopoles on UAV for RX	40	Fixed wing, 101	520 – 1952, 20, 1000 – 54390	1.5-48	PL, PDP, RMS-DS, K-factor, tap probability and statistics (power, delay, duration) in TDL model
[80]	rural, suburban	OFDM	0.97	10	1 monopole antenna on GS for TX, 1 monopole on aircraft for RX	37	Fixed wing, 235	11000, 23, 350000	0-45	PL, PDP, DPP
[81]	rural, suburban, urban, forest	FMCW	5.06	20	1 monopole on UAV for TX, 1 patch antenna on GS for RX	30	Fixed wing, 50	-, 0, 25000	-	CIR, PG, RSS
[82]	Urban	MSK	2.3	6	1 Whip antenna on UAV as transceiver, 1 patch antennas as transceiver on GS	33	Fixed wing, 50	800, 0.15, 11000	4.15-86	RSS
[83]	Urban, suburban, rural	GSM, UMTS	0.9, 1, 9-2, 2	-	Transceiver on balloon and GS	41.76	Captive balloon	450, -, -	-	RSSI, handover analysis
[59]	Urban, hilly, ocean	OFDM	2.4	4.375	4 whip antennas on AV for TX, 4 patch antennas on GS for RX	-	Fixed wing, 120	3500, -, 50000	-	Eigen values, beam-forming gain
[62]	Rural	PRN, BPSK	0.915	10	2 helical antennas on AV for TX, 8 at GS for RX	44.15	Fixed wing, 36	200, -, 870	13-80	CIR, P_R , RMS-DS, spatial diversity
[60]	-	OFDM	5.28	-	4 omni-directional on UAV for TX, 2 on GS for RX	18	Fixed wing, 17.88	45.72, 4.26, -	-	P_R , RSSI
[61]	Urban, open field	OFDM	5.24	-	2 omni-directional on UAV for TX, 2 on GS for RX	20	Quad-copter, 16	120, 2, 502.5	-	RSSI
[84]	Open field	OFDM	5.24	-	3 omni-directional on UAV for TX, 3 on GS for RX	20	Quad-copter, 16	110, 3, 366.87	10-85	RSS
[85]	-	IEEE 802.15.4	2.4	-	On board inverted F transceiver antenna on UAV and GS	0	Hexacopter, 16	20, 1.4, 120	-	RSSI
[44]	Suburban	Wifi, 3G/4G	-	-	Transceiver on UAV and GS	-	Hexacopter, 8	100, -, -	-	P_R , RTT of packets
[86]	Forest (anechoic chamber)	-	8-18	-	Spiral antennas on TX and RX	-	-	2.3, 0.6, 2.85	26-45	P_R
[87]	Open area	Mod. sig.	5.8	-	2 Monopole, 1 horn on UAV for TX, 2 on GS for RX	-	Fixed wing,-	150, 0, 500	-	P_R
[88]	Open area/foliage	802.11 b/g	5.8	-	1 omni-directional on GS for TX, 4 on UAV for RX	-	Fixed wing, 20	75, .2, -	-	Diversity performance
[89]	Urban/suburban, open field, foliage	CW	2.00106, 2.00086	-	2 monopoles on UAV for TX, 2 on GS for RX	27	Gondola airship, 8.3	50 and above, 1.5, 2700	1	P_R
[90]	Urban, rural, open field		0.915	-	1 omni-directional antenna on UAV for TX, 1 on GS for RX	-	Quad-copter,-	-, 13.9, 500	-	RSSI, PL
[91]	Sea	PRN	5.7	-	Omni-directional on AV for TX, 2 directional antennas at GS for RX	40	Fixed wing AV,-	1830, 2.1, 7.65, 95000	-	PL
[57]	Urban	CW	2.05	-	1 monopole on AV for TX, 4 on GS for RX	-	Aerial platform,-	975, -, -	7.5-30	PDP, RMS-DS, MPCs count, K-factor, PL
[71]	Near airport	CW	5.75	-	Directional antenna on GS for TX and omni-directional on AV for RX	33	Fixed wing AV,-	914, 20, 85000	80	P_R , Fading depth, K-factor, PL
[92]	Urban, hilly	Chirp	5.12	20	1 monopole antenna on GS for TX and 1 omni-directional on AV for RX	40	Fixed wing AV, 293	11000, 18, 142000	(-16)-5	PDP

The most common technique of measuring the instantaneous distance is by using GPS traces on both the UAV and GS, but of course GPS devices have accuracy limitations and navigation signals may also be susceptible to interference in different flying zones.

C. AG Propagation Scenarios

A typical type of terrestrial channel sounding equipment, a vector network analyzer, cannot be used for UAV based AG channel sounding due to payload constraints, physical synchronization link requirements, and UAV mobility [97]. Therefore,

TABLE IV
LITERATURE ON UAV AG PROPAGATION CHARACTERISTICS FOR FIVE DIFFERENT FLIGHT ENVIRONMENTS

Ref.	Scenario	Characteristics of scenario	Important factors
[44], [53], [57], [68], [72], [78], [82]	Urban/suburban	Ratio of land area vs ratio of open to built-up area, distribution of building sizes and heights, distribution of ground terminals (vehicles, pedestrians), distribution and characteristics of vegetation, water bodies, etc.	Material of buildings and rooftops
[61], [62], [71], [80], [84], [87], [88], [90]	Rural/open field	Type and density of vegetation, distribution and sizes of the sparse buildings	Surface roughness, soil type, and moisture content
[75], [81], [92]	Hilly/mountainous	Terrain heights and slopes, distribution and type of vegetation, distribution and sizes of buildings	Ground slope, ground roughness
[81], [86], [89]	Forest	Density and types of foliage, and height distributions	Leaves and branches distribution
[54], [58], [74], [91]	Over water	Water type (sea or fresh), distributions and sizes of water surface objects (boats, platforms, etc.), distributions of littoral objects (buildings, water tanks, etc.), and water surface variation (e.g., sea state)	Modified reflection coefficient as compared to ground, ducting effect in case of over sea

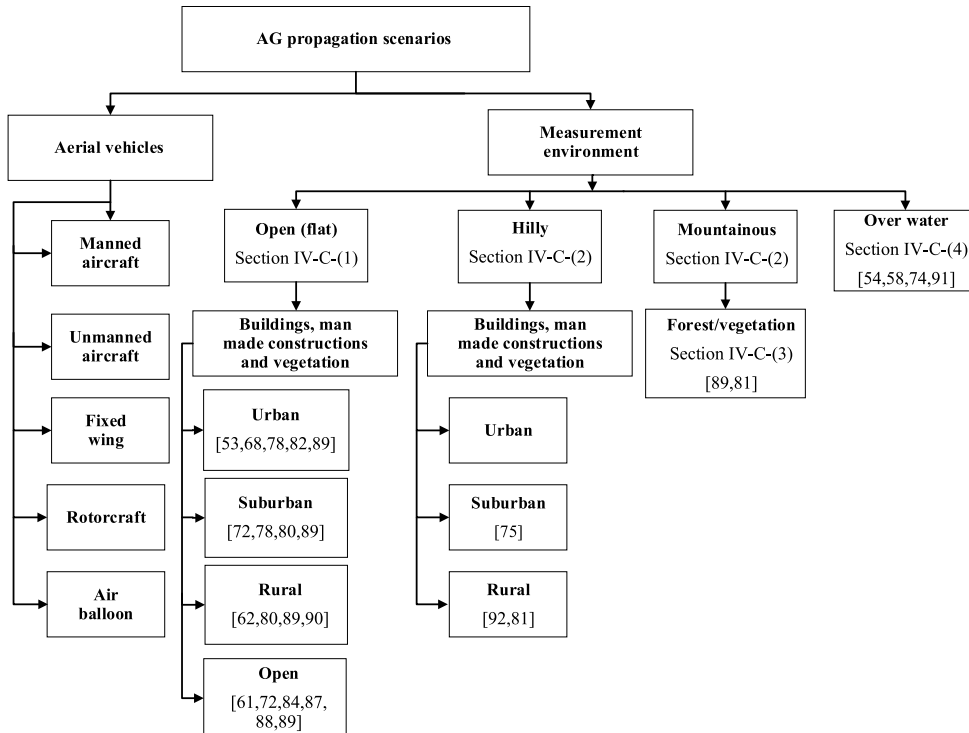


Fig. 2. Measurement scenarios for UAV AG propagation channel.

channel sounding for both narrow-band and wide-band channels using impulse, correlative, or chirp sounding techniques are employed, where the RX is typically on the ground due to payload and processing constraints.

Proper selection of channel measurement parameters in a given environment is critical for obtaining accurate channel statistics for a given application. The AG propagation environment is generally classified on the basis of the terrain type, namely flat, hilly, mountainous, and over water. A particular terrain can have a given cover, e.g., grass, forest, or buildings. The most widely accepted terrain cover classification is provided by the International Telecommunication Union (ITU) [98]. In this survey we classify the cited measurement scenarios as open (flat), hilly/mountainous, and over water. Each scenario can be subdivided on the basis of the terrain cover as shown in Fig. 2.

For any environment, different types of radio controlled UAVs can be used. Balloons or dirigibles are simple to operate

but do not have robust movement characteristics. The non-balloon UAVs can be broadly classified as fixed wing and rotorcraft. The fixed wing UAVs can glide and attain higher air speeds and generally travel farther than the rotorcraft, but rotorcraft are more agile, e.g., most can move straight vertically. Rotorcraft also have the ability to hover, which is not possible for nearly all fixed wing UAVs. The UAV AG propagation scenarios in different environments with particular characteristics are described in Table IV. In the rest of this subsection, we review the different AG measurement scenarios depicted in Fig. 2.

1) *Open Space*: A major part of the literature on AG propagation covers open (flat) terrain. This open terrain can have different terrain covers that affect the channel characteristics. One of the major terrain cover types is buildings. The distribution of building sizes, heights, and their area-wise densities allows sub-classification into urban, suburban and rural areas as depicted in Fig 2. In case of urban and suburban areas,

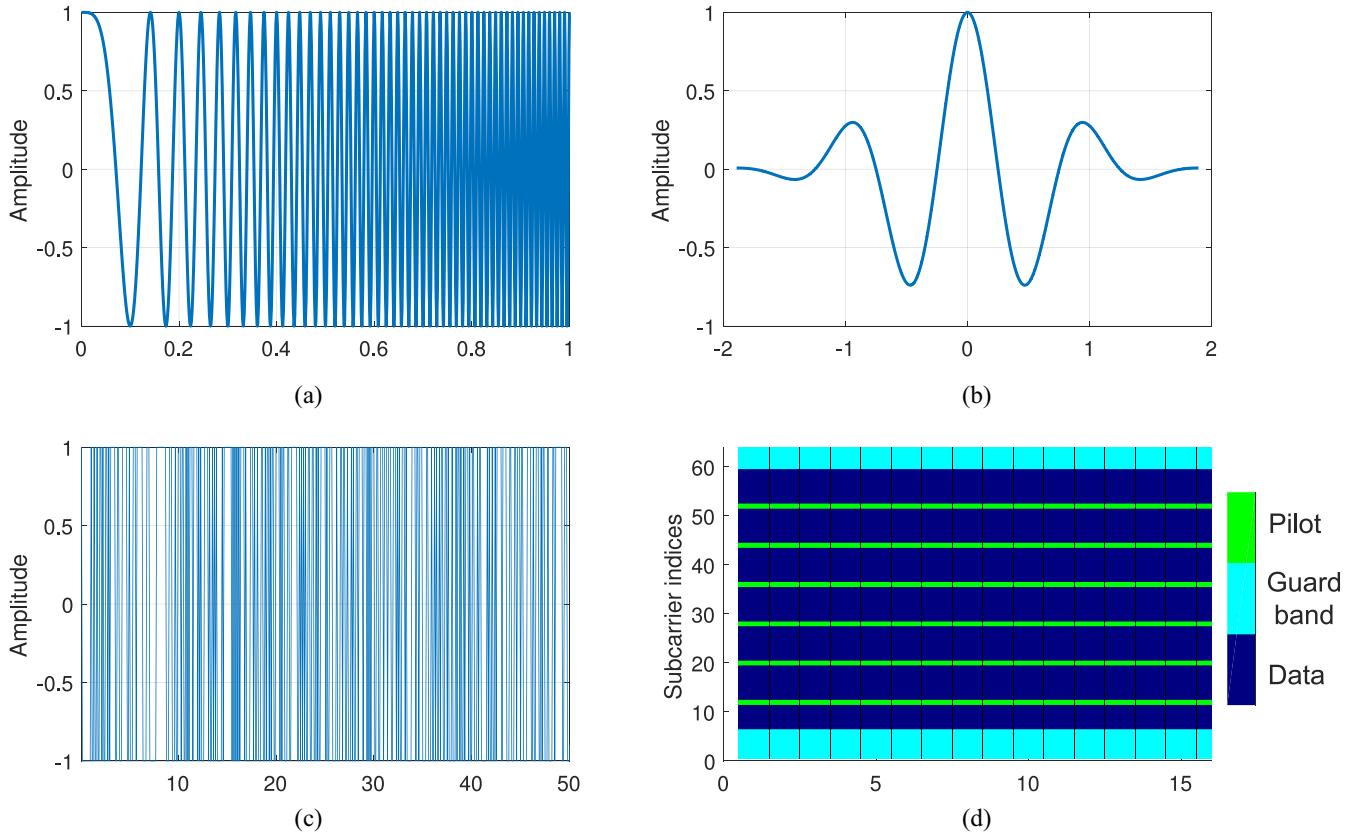


Fig. 3. Sounding signals (a) Chirp signal, (b) Short duration Gaussian pulse sounding signal at center frequency of 1 MHz and fractional bandwidth of 60%, (c) PRN sequence of polynomial degree 10 shown half of the overall period, (d) OFDM sounding signal resource mapping with 64 sub-carriers, 16 symbols and 6 pilots.

there is a higher concentration of man made structures in a given space, e.g., buildings, roads, bridges, large signs, etc. The distribution (and composition) of these complex scatterer structures can strongly influence the channel characteristics. In rural areas, typically buildings are sparse, and of lower height than in urban settings, although large warehouses and other structures could yield strong MPCs.

2) *Hilly/Mountainous*: The hilly/mountainous terrain is characterized by uneven ground heights; equivalently, a large standard deviation of terrain height. The propagation PL in hilly and mountainous areas will mostly follow the two ray model with adjustments due to surface roughness, and potentially reflections from smooth sections of mountain slopes or an occasional large building. The PL over or beyond terrain obstructions can employ established models for diffraction, e.g., [99] but with first Fresnel zone clearance between the TX and the RX, PL is close to free space [75], [76]. Channel dispersion, typically quantified by the root mean square-delay spread (RMS-DS), is generally smaller than in urban/suburban environments [76] but can be large if a strong reflection occurs from a large and distant mountain slope. Generally, hilly and mountainous settings present fewer reflections than more populated regions because of the absence of large numbers of nearby scatterers.

3) *Forest*: There are few comprehensive studies covering AG propagation in forests, especially with UAVs, although there are numerous publications for *roadside* shadowing for

satellite channels, e.g., [100]–[102]. In these studies, propagation effects—typically attenuation—from particular volumes of trees, along with temporal fade statistics are analyzed for long range AG communications. Generally for AG propagation with a GS within a forest, the channel characteristics are dominated by the type and density of trees. Small UAVs within a forest experience different scattering characteristics depending upon height, e.g., the scattering near the tree trunk will be different from that near the tree crown [86]. The scattering is also dependent on the type and density of leaves and branches of the trees, and hence for deciduous trees, can vary seasonally.

4) *Water/Sea*: The AG propagation channel for over water settings is similar to that for open settings, with different surface reflectivity and roughness than ground. The PL can be represented using a two ray PL model, with variations attributable to surface roughness (see small-scale fading in the following section). The RMS-DS in this case is generally smaller than in environments with a large number of obstacles (urban, suburban), although if large objects are on or just off shore, these may produce significant reflections and large delay spreads if geometry permits.

In case of propagation over sea, the height of waves in a rough sea can introduce additional scattering and even diffraction for very low height stations on the sea. An interesting propagation phenomenon that can also occur over sea is ducting, where anomalous index of refraction variation with

height results in propagation loss less than that of free space [91]. This phenomenon is dependent on frequency and meteorological conditions, and is thus typically addressed statistically [103].

D. AG Channel Sounding Waveforms

As noted in [67], [92], common channel sounding signals include short pulses (approximately impulses), direct sequence spread spectrum (DS-SS) signals for correlative processing, linearly varying frequency modulated (chirp) signals, and multi-tone signals. Different example sounding signals are shown in Fig. 3 representing a chirp signal, RF Gaussian pulse, pseudo-random number (PRN) sequence, and OFDM sounding signals. These sounding signals have been used in different measurement campaigns summarized in Table III in different AG channel measurement scenarios given in Fig. 2. Short duration pulses are direct approximations of input impulses and MPCs can be directly measured in the time domain (e.g., via a sampling oscilloscope). The primary drawback is generation of sufficient pulse energies to reach long distances, and large peak-to-average power ratios (PAPR). The DS-SS signaling uses pseudo-random (PR) sequences to generate a wideband noise-like signal that is demodulated with a sliding (or sometimes a stepped) correlator; this correlation processing yields an estimate of the channel impulse response (CIR). The DS-SS technique can use binary phase shift keying transmission and with modest filtering this yields a low PAPR. Chirp sounding has the advantage of high frequency resolution and the potential to sweep over large frequency ranges; PAPR can be the ideal value of unity. The chirp technique yields the channel transfer function, from which the CIR is obtained via inverse Fourier transformation.

Another popular technique is the use of a multitone signal, with the idea of sampling the channel transfer function. This is in essence an OFDM based channel sounding. One advantage of using OFDM sounding is that known data can be used for sounding, hence allowing some data transmission along with channel sounding [104]. The OFDM signals have the advantage of a flat spectrum but of course a *sinc* ($\sin(x)/x$) delay domain response and a large PAPR. Details on these various sounding signals can be found in the literature, e.g., [105].

Different carrier frequencies can be used to sound the AG channel and in principle this is completely arbitrary, but most measurements aim at frequency bands in which UAV use is at least possible. Measurements have ranged from 100 MHz to 18 GHz with perhaps most of the measurements carried out in the 5 GHz band (5.06 GHz - 5.8 GHz). Similarly, sounding signal bandwidth varies, from very narrow-band to several tens of MHz or more. In [72], UWB channel sounding with a bandwidth of 2.2 GHz was used, yielding sub-nanosecond time resolution.

E. Elevation Angle Effects

It is important to consider the effect of elevation angle for UAV AG communications, as it is for satellite communications. This is in contrast to the case of terrestrial communications, where the effect of the elevation angle is less significant due to (1) smaller heights of TX and RX, and

(2) NLOS communication for a substantial fraction of users. The effect of elevation angle can also vary with the type of antennas used. If the communication is directional, and the UAV and GS beams are aligned, then the effect of the elevation angle is negligible. However, if the communication is omni-directional, then the effect of the antenna gain at higher elevation angles will be significant.

In [106], [107], the effect of elevation angle at different UAV altitudes for different antenna orientations was discussed. The gain of the omni-directional dipole antenna in the elevation plane was modeled as a trigonometric function of physical elevation angle between the UAV and the GS. It was shown that the effect of the elevation angle on the received power was essentially deterministic when the UAV is hovering, but was not as easily modeled when the UAV was in circular motion around the ground RX.

The effect of elevation angle on UAV AG omni-directional communications at 28 GHz was discussed in [108]. It was observed that received power was mainly dependent on the elevation angles of the LOS and ground reflected components (as they were the strongest). The received power was a function of link distance and elevation angle, with the latter a strong function of antenna gain: for some distances and angles, antenna gain effects dominated, but at larger distances the antenna gain was less significant than the effect of attenuation (FSPL) with distance.

Similarly, in [93], the received power was shown to follow a two ray model. It was also shown that the received power and RMS-DS dependence on UAV height is a function of the specific propagation environment. For example, in a rural area, the effect of ground scatterers was negligible at higher UAV altitudes, whereas for an urban area, the effect of scatterers was observed at higher UAV altitudes. Similar results were reported for TOA, angle of arrival, and angle of departure of MPCs in [108], where larger temporal and angular spreads were observed at UAV heights comparable to the scatterer heights.

V. UAV AG PROPAGATION MEASUREMENT AND SIMULATION RESULTS IN THE LITERATURE

Several types of channel statistics are useful for characterizing the channel for different applications. For AG propagation, the channel statistics are similar to those gathered for terrestrial channels. In general, propagation channels are linear and time varying, but can sometimes be approximated or modeled as time-invariant. For linearly time-varying channels, the CIR or its Fourier transform, the time varying channel transfer function (CTF), completely characterizes the channel [53], [54], [57], [58], [62], [68], [73]–[79], [92]. As noted, due to relative motion of the UAV, the AG channel may be stationary only for small distances [58]. Thus, *stationary distance* needs to be taken into account when estimating the channel statistics [54], [109], [110].

Another higher-level parameter that has been used by some researchers to characterize the quality of the AG propagation channel is throughput, but of course this is highly dependent upon the TX and the RX implementation, and parameters of the air interface, such as the number of antennas and the

transmit power. Hence this measure is of limited use for assessing the AG channel itself. Similarly, for MIMO channels, beam-forming gain, diversity, and capacity of the channel are often estimated. Some commonly reported channel characteristics for AG propagation channels are given in the following subsections.

A. Path Loss/Shadowing

Most of the AG propagation campaigns address PL and if present, shadowing, in different scenarios. For AG channels with a LOS component, PL modeling begins with FSPL; when the earth surface reflection is present (not blocked or suppressed via directional antennas), PL can be described by the well-known two-ray model. Parallel to the developments in terrestrial settings, most of the measurements employ the log-distance PL model where the loss increase with distance is indicated by the PLE. In [72], PL is calculated for open field and suburban areas for different UAV and GS heights for a small hovering UAV. Comprehensive PL measurements in L and C bands were carried out in different propagation scenarios in [53], [54], [58], [73]–[79] as summarized in Table III. The values of PLE were found to be slightly different for urban, suburban, hilly, and over water scenarios, but are generally close to the free-space value of 2 with standard deviation around the linear fit typically less than 3 dB.

In [61], it was observed that the PLEs for IEEE 802.11 communications were different during UAV hovering and moving due to different orientations of the on-board UAV antennas. Therefore, antenna patterns can distort the true channel PL characteristics and removing their effect is not always easy or possible. On the other hand, for the specific UAV configuration used, the resulting PL model is still useful. Typically, PL for LOS and NLOS conditions are provided separately, e.g., [111], where for the NLOS case, there is an additional small-scale (often modeled as Rayleigh) fading term, and a constant reflection term in addition to the LOS PL. Analogously, the LOS models for L- and C-bands can incorporate Ricean small scale effects [58]. In [112], the reported PL is described as a function of the elevation angle between the low altitude platform and GS, θ given as follows:

$$PL = 20 \log \left(\frac{\Delta h}{\sin \theta} \right) + 20 \log(f_{\text{MHz}}) - 27.55, \quad (1)$$

where $\Delta h = h_U - h_G$ is the difference between the height of the low altitude platform (UAV) and the GS, f_{MHz} is the operating frequency expressed in MHz. The argument $\Delta h / \sin \theta$ is simply the link distance expressed as a function of the elevation angle.

PL including shadowing is reported in [57], [68], [71], [72], [113], [114], where we note that in LOS cases without actual obstruction of the first Fresnel zone, the physical mechanism causing PL variation is not actually shadowing but often small-scale effects. In [68], PL and its associated shadowing was attributed to buildings only when the UAV was flying near the ground whereas when flying higher, actual shadowing was not present but variation from small-scale fading still occurred. One can also estimate losses due to “partial” shadowing by conventional methods. For example the shadowing in [113]

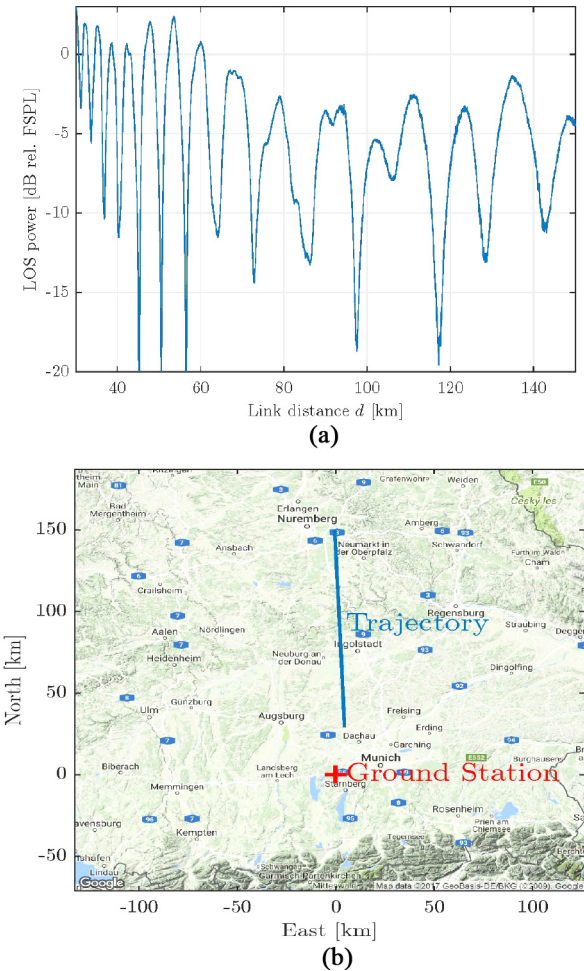


Fig. 4. (a) The LOS signal power variation due to ground multipath propagation. The power is normalized to FSPL, (b) Measurement scenario environment in [115].

was found to be a function of the elevation angle, where the shadowing magnitude was estimated by using the uniform theory of diffraction.

In Fig. 4(a) we show an example for the variation of the LOS signal power due to ground reflected MPCs versus the link distance d . Specifically, this is the *combined* effect of the LOS component and the unresolved ground reflection. The measurements were taken in a rural environment using a 10 MHz signal bandwidth. The GS height h_G was 23 m. The UAV trajectory is shown in Fig. 4(b). During the measurements, the specular reflection point first passed over the roof of a building and then over open grassy fields [115]. From Fig. 4(a) we observe a periodic variation of the received power: an attenuation of the signal by more than 10 dB is not uncommon. These signal fades will of course generally negatively impact the performance of any communication system. For an increasing link distance the frequency of the variation decreases—a direct manifestation of the two-ray model. Thus in such a channel, even for a UAV flying at a high speed a fade can easily last several seconds. It is essential to note that a ground MPC may not always be present, e.g., for the case when the ground is a poorly reflecting ground surface, or the surface is very rough relative to the signal wavelength.

The PL provides complete information on link attenuation, but another indirect parameter often used for channel attenuation estimation is RSS. In [60], [61], [84], RSS indicator data for an AG propagation channel based on IEEE 802.11a transmissions with different antenna orientations was provided. Data on fluctuations in RSS due to multipath fading from tall building reflections was provided in [81], where the RSS was found to decrease due to polarization mismatch between the TX and the RX antennas when the aerial vehicle made a banking turn. The accuracy of RSS values in commercial products can vary considerably, so when these are used, care should be taken in calibration.

B. Delay Dispersion

The power delay profile (PDP) is the “power version” of the CIR. This can be computed “instantaneously,” or more traditionally, as an average over a given spatial volume (where the channel can be considered WSS). Various AG propagation studies in different environments have measured PDPs, and via the PDP the most common estimate of the delay-domain dispersion is estimated: the RMS-DS. Other dispersion measures such as the delay window or delay interval are also sometimes reported. Statistics for the RMS-DS itself are often computed, e.g., in [57], mean RMS-DS values for different elevation angles were reported. As generally expected from geometry, the RMS-DS was found to decrease as elevation angle increases. In [72] PDPs were measured for open areas, suburban areas, and areas covered with foliage.

The Saleh-Valenzuela model, originally developed for indoor channels, is sometimes used to model the PDP when MPCs appear grouped or “clustered” in delay. This model specifies the MPCs by such clusters, and the number of clusters is different for different environmental scenarios. PDPs were measured for different environments in [54], [74]–[79], and resulting RMS-DS statistics were provided. As expected, the delay spread was found to be dependent on the terrain cover with maximum delay spread values of 4 μs for urban and suburban settings. The largest RMS-DS values generally occur when there are large buildings that can provide strong MPC reflections. For hilly and mountainous terrain, maximum RMS-DS values of 1 μs for hilly regions and 180 ns for the mountainous terrain were reported. In over water settings, the maximum RMS-DS value reported was 350 ns. Again, in all these settings cited here, a LOS component was present between GS and UAV, hence for the majority of the time, RMS-DS was small, on the order of a few tens of nanoseconds. In [116], a finite-difference time domain model for the electric field propagating at very low heights over sea was developed. An RMS delay spread model for VHF to 3 GHz was presented, with RMS-DS a function of wave height.

C. Narrowband Fading and Ricean K-Factor

Small scale amplitude fading in AG propagation channels usually follows a Ricean distribution due to the presence of a LOS component. The Ricean *K*-factor is defined as the ratio of dominant channel component power to the power in the sum of all other received components. The *K*-factor is often used to

characterize the AG channel amplitude fading. In [57], as generally expected, the authors found that the *K*-factor increased with increasing elevation angle. The Ricean *K*-factor as a function of link distance was given in [71], during multiple phases of flight (parking and taxiing, take off and landing, and en-route). The en-route phase showed the largest *K*-factor, followed by take off and landing, and parking and taxiing. In [86], it was observed that the *K*-factor will differ with different types of scattering trees: values of *K* ranging from 2 dB to 10 dB were reported.

The *K*-factor was measured for both L-band and C-band AG propagation in [53], [58], [76], [79] for urban, suburban, hilly and mountainous settings, and also for over fresh water and sea scenarios. The mean values of *K*-factor for urban areas were reported to be 12 dB and 27.4 dB for L-band and C-band respectively. The mean *K*-factor values for hilly and mountainous terrain were reported to be 12.8 dB and 29.4 dB for L-band and C-band respectively, whereas for over sea settings, *K*-factor mean values for L-band and C-band were found to be 12.5 dB and 31.3 dB, respectively. Worth pointing out is that in these “strong LOS” channels, the *K*-factor does not strongly depend on the GS environment. Also observed was that the C-band *K*-factor was larger than the L-band *K*-factor in all environments. This is attributable to two causes: first, the C-band measurement signal bandwidth was larger than that of L-band, ameliorating fading, and second, for any given incident angle and surface roughness (e.g., ground, or ocean), as carrier frequency increases, the surface roughness with respect to the wavelength also increases, and hence incident signals are scattered in multiple directions rather than being reflected in a single direction (toward the RX). With fewer and/or weaker MPCs at the higher frequency, the *K*-factor is larger.

D. Doppler Spread

The Doppler effect is a well-known phenomenon for wireless mobile communications. Considering AG propagation with UAVs in a multipath environment, if we let ϕ_i represent the angle between the aircraft velocity vector and the direction from which the i^{th} MPC is received, the Doppler frequency shift of this i^{th} MPC is $f_d^i = \frac{v \cos \phi_i}{\lambda}$, where v is the UAV velocity, and λ is the wavelength of the radio wave. (We assume here that the GS is motionless, else a more general formulation for the Doppler shift must be used.) If MPCs are received with different Doppler frequencies this phenomenon produces spectral broadening, called Doppler spread.

In [34], [71], simulations were used to find the Doppler shift and its effect on the channel at different phases of flight (parking and taxiing, en-route, and take off and landing). Doppler spread in a multipath environment implementing OFDM systems was considered in [67], where arriving MPCs were observed to have different frequency offsets. In such a case, if the RX CFO synchronizer cannot mitigate the effect of these different frequency offsets, this results in ICI. In [47], a mitigation technique for Doppler shift was proposed for the case where the UAV is relaying between two communication nodes. The UAV acts as a repeater that provides the required frequency shift to mitigate the Doppler effect. A three dimensional AG Doppler delay spread model was provided

in [46] for high scattering scenarios. Doppler spread for AG propagation is also discussed in [62], [66], [72], [73], [92].

E. Throughput and Bit Error Rate Statistics

Other than the channel characteristics reviewed earlier, there are other performance indicators that can be measured. Two of these are throughput and bit error ratio (BER) with particular communication technologies. As with RSSI measurements, these are useful for the particular technology and environment in question, but may offer very little that is directly relevant to modeling the AG channel. The throughput of an AG propagation channel was investigated in several studies, most commonly using the IEEE 802.11 protocol. Throughput analysis using different versions of the IEEE 802.11 protocol were carried out in [60], [61], for different antenna orientations, propagation distances, and UAV elevations. A throughput analysis of IEEE 802.11n was carried out in [42], where—as expected—it was found that throughput is directly dependent on the modulation and coding scheme. Throughput analysis for data relaying and ferrying for an AG propagation channel was carried out in [43]. It was observed here that mobile relaying can achieve more than twice the throughput of static relaying for a given delay tolerant system.

Some results for BER as a function of signal-to-noise-ratio (SNR) for AG propagation channels are available in the literature to compare the performance of different implementation schemes. In [117], BER was measured against SNR for different modes of LDACS1, as a function of distance and for different phases of flight. A similar study was conducted in [118], where BER was measured against SNR for an over sea AG propagation channel with distance measuring equipment (DME) co-channel interference present. In [119], BER versus SNR analysis was performed for different flight route phases for different values of Ricean K -factor. BER versus SNR analysis was performed in [70] for comparing the effect of presence and absence of ICI for an IEEE 802.11a OFDM system in the presence of additive white Gaussian noise (AWGN).

F. Effects of UAV AG Measurement Environment

The different AG propagation channel measurement campaigns can be broadly classified based on terrain, terrain cover and sounding signal characteristics. In this subsection, we will provide a brief overview and comparison of different approaches.

1) *Urban/Suburban*: UWB AG propagation channel measurements were provided in [72], using PRN sounding pulses. These measurements are unique as large bandwidth AG channel measurements are not available in the literature. However, the link distance and UAV heights considered are small due to small transmit power allowed by the FCC. Buildings over a flat terrain in the suburban area with an average height of 12 m, resulted in additional reflections and respective shape of the PDP as compared to the open area. In [68], a continuous wave (CW) narrowband sounding signal with a center frequency of 2 GHz was used in an urban scenario. There were uniformly built buildings in the urban area with an average height of 22 m. Second order channel fading statistics of

level crossing rate and average fade duration were analyzed for different heights and horizontal distances of the aerial platform from the GS. This work is unique as the second order channel fading statistics for AG propagation using UAVs are rarely available in the literature. However, the velocity of the aerial platform considered was very less. Additionally, it would have been more interesting if second order statistics were compared at different UAV velocities in the same environment.

In [53], [78], wideband AG propagation channel measurements were reported for suburban and urban areas in the L-band and C-band. It was observed that reflections from high rise buildings resulted in increase in the RMS-DS. The large scale and small scale fading at two different frequency bands in the similar environment were found to be different. In [57], wideband CW sounding signal at a center frequency of 2.05 GHz was used in an urban area like environment of a university campus. There were 4 to 6 story tall buildings and the terrain was rolling. It was observed that the RMS-DS increased with decreasing the elevation angle, whereas the number of MPCs remain the same, suggesting that at lower elevation angles the MPCs have larger power. In both [57] and [68], measurements were performed in the approximately similar environments and at same center frequency, only the bandwidths were different. However, the multipath fading distribution in [57] was found to be Rayleigh/Ricean, whereas for [68], it was found to be Loo.

2) *Rural/Open Field*: In [80], a rural environment similar to an airport with large and small buildings and open grassy fields was considered for channel measurements. Wideband OFDM channel sounding was performed in the L-band at a center frequency of 970 MHz. These channel measurements were preformed at an aerial height up to 11 km. Due to higher altitude, the tropospheric effects were also considered. In addition, interference effects such as from DME were also taken into account. A link distance of 350 km was considered that is much larger than available in the literature. In [71], channel measurements were carried out near airports using a wideband CW signal centered at 5.75 GHz. Channel measurements were obtained for different flight scenarios of parking and taxiing, en-route, and take off and landing. Received power and small scale fading statistics at different flight scenarios were analyzed, where during taxiing and take-off higher RMS-DS, K -factor and Doppler shift were observed. In [90], measurements were conducted in order to explore the feasibility of fixed cellular network for telemetry and control of UAVs, particularly, in the perspective of radio propagation at shorter distances in the sky as compared to terrestrial. The center frequency of operation was 0.915 GHz. Comparisons of AG measurement results with the COST-231-WI were provided showing that received power from measurements was overestimated by COST-231-WI model.

In [87], channel measurements were carried out in an open field using a modulated signal centered at 5.8 GHz, with two TXs operating at slightly different frequencies. A MIMO configuration was used for channel measurements with directional and omni-directional antennas. It was observed that multipath interference can be reduced using directional antennas. Additionally, using multiple antennas on-board UAVs can

provide robustness against received power fluctuations due to varying antenna orientations on the aerial platform. However, no propagation model was provided. In [62], wideband PRN, binary phase shift keying (BPSK) sounding signal was used at a center frequency of 0.915 GHz. Analysis of spatial diversity for MIMO signaling was carried out. Additionally, near field scattering region analysis around the UAV and the GS were carried out. It was observed that additional spatial diversity could be obtained from objects near the GS. The MPCs were reported to be sparse similar as observed in [108], though at a lower frequency.

3) *Mountains/Hilly, Over Sea, Forest*: In [92], AG propagation channel measurements were performed in a near mountainous area using a wideband chirp signal at a center frequency of 5.12 GHz. The overall terrain was flat with some nearby mountains resulting in moderate MPCs. The channel characteristics were largely dictated by the LOS component. The effect of airframe shadowing were also observed. In [75], [76] channel measurements were performed in the L-band and C-band in an urban hilly area. Curved earth two ray (CE2R) model with weaker reflections and scattering from the hilly terrain and terrain cover were observed. Additionally, multiple clusters of MPCs due to reflections from hills and buildings on hills were observed. In [81], a wideband frequency modulated continuous wave (FMCW) signal centered at 5.06 GHz was used for channel measurements in a hilly area. RSS fluctuations due to MPCs from nearby buildings were reported. In the measurement campaigns of [75], [76], [81], the frequency bands were close in approximately similar environments. However, different results were observed, e.g., in [76], a better fitting with CE2R model was observed in the C-band from the received power however, a free space attenuation fitting was observed in [81] for one of the flight tracks.

In [91], wideband channel measurements were performed using PRN sequence at a center frequency of 5.7 GHz over the sea. Multipath channel statistics were analyzed at different heights of the aerial platform. It was observed that the CIR can be represented using a 3 ray model. Elevation and evaporation ducting effects were observed that resulted in reduction of the attenuation. Over sea measurements were also carried out in [54], [58], [74], for over sea and near harbor areas. A dominant two ray model was observed for the all the cases. No ducting effect was observed over the sea for these measurements as opposed to [91].

In [86], an AG propagation scenario through a forest was imitated in an anechoic chamber using different heights of the TX and the RX and with different species of trees. Channel measurements were carried out in the X-band and Ku-bands. Different diffuse scattering regions from different parts and respective species of the trees were observed, resulting in corresponding small scale fading statistics. Similar results were observed in [72], where foliage in the form of a medium sized tree obstructed the direct LOS path between the UAV and the GS resulting in peculiar small scale fading due to diffraction and scattering from different parts of the tree. In [89], channel measurements were carried out using CW sounding signal centered at 2 GHz. Received power was measured in different propagation environments

including woods, where the shadowing from the woods was found to be significantly different than obtained from the buildings.

G. Simulations for Channel Characterization

Apart from measurement campaigns for AG propagation channel modeling, some simulation based channel characterizations are also available in the literature, where the real time environmental scenarios are imitated using computer simulations. Simulations in urban/suburban areas were performed in [69], [112], [114], [119]. The antenna considered in these environments was omni-directional. Different carrier frequencies 200 MHz, 700 MHz, 1 GHz, 2 GHz, 2.5 GHz, 5 GHz, and 5.8 GHz were covered for AG channel characterization in the urban/suburban environments, and different heights of UAVs, ranging from 200 m to 2000 m were considered. The PL (from simulated RSS) was estimated. Over sea based channel simulations were carried out in [116], where a channel simulator imitating the sea environment was developed. Carrier frequencies from 3 kHz - 3 GHz were used, with the TX and the RX placed 3.75 m above the sea surface. The main goal of the study was to quantify sea surface shadowing for the marine communication channel using UAVs. The channel characteristics of PL and RMS-DS were modeled based on the sea surface height.

In [118], simulations were conducted in environmental scenarios consisting of over sea, hilly, and mountainous terrain. Performance of AG communications using filter bank multi-carrier (FBMC) modulation systems and LDACS were compared. The results showed that FBMC has better performance than LDACs, especially in the presence of interference from DME signals. In the presence of the AG channel, the FBMC and LDACS performance is comparable. Other simulations of communication systems employed over AG propagation channels, for particular simulation scenarios, are also available in the literature [47], [67], [120].

In [121], the effect of the UAV height for optimal coverage radius was considered. It is observed that by adjusting UAV altitude, outage probability can be minimized: a larger “footprint” is produced with a higher UAV altitude, but of course increased altitude can increase PL. An optimum UAV height is evaluated that maximizes the coverage area for a given SNR threshold. The Ricean K -factor was found to increase exponentially with elevation angle between UAV and GS, given as $K = c_1 \exp^{c_2 \theta}$, where c_1 and c_2 are constants dependent on the environment and system parameters. The relation between minimizing outage probability or maximizing coverage area for a given SNR threshold is solved only based on PL without considering the effect of scatterers in the environment. The consideration of geometry of scatterers in the analysis would of course make it more robust and realistic.

VI. UAV AG PROPAGATION MODELS

The UAV AG propagation measurements discussed in the previous section are useful for developing models for different environments. In the literature, UAV AG propagation channel models have been developed using deterministic or statistical

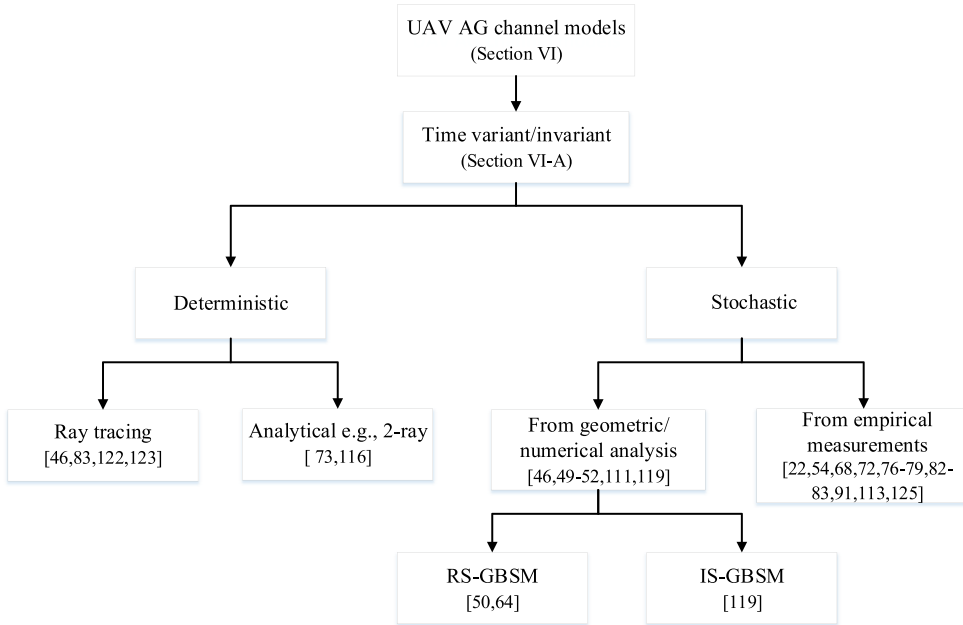


Fig. 5. AG channel model characterization.

approaches, or their combination. These channel models can be for narrow-band, wide-band, or even UWB communications. Complete channel models include both large scale and small scale effects. In this section, we categorize AG propagation channel models in the literature as shown in Fig. 5, and review some of the important channel models.

A. AG Propagation Channel Model Types

Time-variant channel models can be obtained via deterministic or stochastic methods or by their combination. The deterministic methods often use ray tracing (or, geometry) to estimate the CIR in a given environment. These deterministic channel models can have very high accuracy but require extensive data to characterize the real environment. This includes the sizes, shapes, and locations of all obstacles in the environment, along with the electrical properties (permittivity, conductivity) of all materials. Hence such models are inherently site-specific. They also tend to require adjustment of parameters when comparing with measurement data. Since ray tracing based techniques employ high-frequency approximations, they are not always accurate. They are not as accurate as full wave electromagnetic solutions, e.g., the method of moments and finite difference time domain methods for solving Maxwell equations [122], but ray tracing methods are of course far less complex than these full-wave solutions. Such deterministic simulators are also very complex when they are used to model time varying channels. Ray tracing was used in [46], [83], [112], [114], [123], [124] for different fully deterministic AG propagation scenarios.

The models in [54], [76], [78] are a mix of deterministic and stochastic models (sometimes termed quasi-deterministic). Specifically, the LOS and earth surface reflection are modeled deterministically via geometry, and the remaining MPCs are modeled stochastically, with parameter distributions (for MPC

amplitude, delay, and duration) for each environment based on a large set of measurement data.

Purely stochastic channel models can be obtained either from geometric and numerical analysis without using measurements or they can be wholly empirical. Early cellular radio channel models, e.g., the COST 207 models, are examples of the latter. These types of models are becoming less and less common over time though, as incorporation of known physical information is shown to improve accuracy, and the greater model complexity is no longer prohibitive because of continuing advances in computer memory capacity and computational power. Geometric based channel models for AG propagation generally require three spatial dimensions to be accurate. The associated velocity vector for UAV motion in space also requires three dimensions, although 2D approximations can often be very accurate. In order to model the scatterers around the GS, two elliptical planes intersecting a main ellipsoid were considered in [51], [52], [111], [119], where the MPCs are defined by the ellipsoid and the two elliptical planes. Scatterers are considered to be randomly distributed on two spheres surrounding the TX and the RX in [50]. In [49], [64], the distribution of scatterers around the GS is modeled using a three dimensional cylinder.

The geometry-based stochastic channel models (GBSCMs) can be further classified into regular shaped GBSCMs (RS-GBSCMs) or irregular shaped GBSCMs (IS-GBSCMs). For RS-GBSCMs, the scatterers are assumed to be distributed on regular shapes, e.g., ellipsoids, cylinders, or spheres. These models often result in closed form solutions, but are of course generally unrealistic. In contrast, the IS-GBSCM distributes the scatterers at random locations through some statistical distribution. The properties of the scatterers in both cases are generally defined beforehand. In some cases, authors assume a large number of scatterers a priori, and via the Central Limit Theorem, obtain a Ricean amplitude distribution to obtain

TABLE V
REVIEW OF EXISTING LITERATURE ON LARGE SCALE AG PROPAGATION AND THE PATH LOSS PARAMETERS IN THOSE PAPERS

Ref.	Scenario	Path (LOS/NLOS)	Model type	PLE (γ) or (α, β) parameters	Intercept PL_0 (dB)	σ (dB)
[72]	Suburban, open field	LOS,OLOS	log-distance PL, Eq. (1),(2)	$\gamma : 2.54 - 3.037$	21.9 – 34.9	2.79-5.3
[22]	Lightly hilly rural (for $h_U = 120$ m) for other values of the height, see Table II in the paper	LOS	log-distance PL (alpha-beta model), Eq. (2)	$\alpha = 2.0, \beta = -35.3$	-	3.4
[81]	Urban, suburban, rural	-	FSPL	-	-	-
[82]	Urban	-	FSPL, Eq. (1)	-	-	-
[78]	Urban, suburban	LOS	Log-distance PL, two ray model, Eq. (1)(2)	$\gamma : 1.7$ L-band, 1.5 – 2 C-band	98.2 – 99.4 L-band, 110.4 – 116.7 C-band	2.6 – 3.1 L-band, 2.9 – 3.2 C-band
[113]	Urban, suburban	LOS,NLOS	Modified FSPL, Eq. (5)(6)	-	-	-
[61]	Urban, open field	LOS	Log-distance PL, Eq. (1)	$\gamma : 2.2 - 2.6$	-	-
[125]	Urban	LOS,NLOS	Modified FSPL, Eq. (1)(9)(10)(13)	-	-	-
[126]	Urban	-	Modified LUI model, Eq. (1)	-	-	-
[57]	Urban, rural	LOS	Log-distance PL, Eq. (7)	$\gamma : 4.1$	-	5.24
[71]	Near airports	LOS	Log-distance PL, Eq. (1)	$\gamma : 2 - 2.25$	-	-
[84]	Open field	-	Log-distance PL, Eq. (1)	$\gamma : 2.01$	-	-
[85]	-	LOS	Log-distance PL	$\gamma : 2.32$	-	-
[76]	Hilly, mountainous	LOS	Log-distance PL, Eq. (3)	$\gamma : 1.3 - 1.8$ L-band, 1 – 1.8 C-band	96.1 – 106.5 L-band, 115.4 – 123.9 C-band	3.2 – 3.9 L-band, 2.2 – 2.8 C-band
[86]	Forest/foliage	-	-	-	-	-
[58]	Over sea	LOS	Two ray PL, Eq. (1)	-	-	-
[54]	Over water, sea	LOS	Log-distance PL, two ray PL, Eq. (15)(16)(17)	$\gamma : 1.9, 1.9$ over water and sea for L-band, 1.9, 1.5 over water and sea for C-band	104.4, 100.7 over water and sea for L-band, 116.3, 116.7 over water and sea for C-band	3.8 – 4.2 over water and sea for L-band, 3.1 – 2.6 for over water and sea for C-band
[91]	Over sea	LOS	Two ray PL, FSPL, Eq. (2)(3)	$\gamma : .14 - 2.46$	19 – 129	-
[127]	Ensemble of containers, see Table II in the paper	LOS	Dual slope, Eq. (1)(2)(3)	-	-	-

estimates of the CIR based upon some geometry. Alternatively, signal interaction from randomly distributed scatterers can be estimated directly, or with the help of ray tracing software [112], [114], [123]. A non-geometric stochastic channel model (NGSCM) based on a Markov process is provided in [66]. The ground to air fading channel was described by a Markov process that switches between the Ricean and Loo models, depending on the flight altitude.

B. Path Loss and Large Scale Fading Models

As noted, in mostly-LOS AG channels, large scale fading only occurs when the LOS path between UAV and GS gets obstructed by an object that is large relative to the wavelength. Some models for this attenuation mechanism exist (e.g., terrain diffraction, tree shadowing), but not much measurement data for UAV channels obstructed by buildings has been reported. When the LOS path does not get obstructed, the only other truly large-scale effect is the two-ray variation from the earth surface MPC. There are numerous measurement campaigns in the literature for PL estimation in different environments, as summarized in Table V. Large

scale fading models in the literature cover both the PL and shadowing.

1) *Free Space Path Loss Model*: In the majority of the literature, the well-known terrestrial based log-distance PL model with FSPL reference (“close-in,” CI) is used:

$$PL_{CI}(d) = PL_0 + 10\gamma \log_{10}(d/d_0) + X_{FS}, \quad (2)$$

where $L_{CI}(d)$ is the model PL as a function of distance, PL_0 is the PL at reference distance d_0 in free space given by $10 \log [(\frac{4\pi d_0}{\lambda})^2]$, γ is the PLE obtained using minimum mean square error best fit, and X_{FS} is a random variable to account for shadowing, or in the case of LOS channels, the variation about the linear fit. In free space the value of PLE is 2, but as seen from Table V, measured values of PLE vary from approximately 1.5 to 4. One might conceptually divide the path between the UAV and the GS into two components: the free space component above the ground and the remaining *terrestrial influenced* components. When the GS antenna height is well above surrounding obstacles, we expect the terrestrial components to have smaller effect and the PLE is near to that of free space.

2) *Floating Intercept Path Loss Model*: Another PL model used in the literature for large scale fading is floating intercept (FI) [128]. This model is similar to (2), but the FSPL at reference distance is eliminated and the model is dependent on two parameters represented as α and β [22], where α is the slope and β represents the intercept given as

$$PL_{\text{FI}}(d) = \alpha 10 \log_{10}(d) + \beta + X_{\text{FI}}, \quad (3)$$

where X_{FI} is a random variable representing the variation of the PL.

3) *Dual Slope Path Loss Model*: The two PL models discussed above are based on single slope. These models hold in areas where the characteristics of the channel do not change drastically. The two PL models in (2) and (3) have different interpretations. The model in (2) uses a reference distance of typically 1 m from the transmit antenna and find the slope using minimum mean square error, whereas no reference distance is used for calculating the PL in (3) and linear least square error regression is used to obtain the fitting for the data. Additionally, β in (3) is not PLE, as it is not obtained through a free space reference distance near the antenna [129]. At short distances, the model in (3) provides an underestimated PL, whereas it provides an overestimated PL at larger distances [130], therefore, use of CI model in (2) is recommended for all the scenarios. However, in some settings with NLOS paths and complex geometries resulting in higher order reflections and diffractions, these single-slope models can have large regression errors. In such cases, a dual slope (DS) PL model is sometimes used [127], [131]. This model is similar to the FI model, but has two different slopes for different link distance ranges, and can be represented as

$$\begin{aligned} PL_{\text{DS}}(d) \\ = \begin{cases} \alpha_{d_1} 10 \log_{10}(d) + \beta_{d_1} + X_{\text{DS}}, & d \leq d_1 \\ \alpha_{d_1} 10 \log_{10}(d_1) + \beta_{d_1} + \alpha_{d_2} 10 \log_{10}(d/d_1) + X_{\text{DS}}, & d > d_1 \end{cases} \end{aligned} \quad (4)$$

where α_{d_1} , α_{d_2} , are the slopes of the fits for at two link distance ranges separated by threshold d_1 , β_{d_1} is the intercept, and X_{DS} is a random variable representing the variation in the fit.

4) *Log-Distance Path Loss Model*: PL estimates using log-distance models (2) are given in [53], [60], [61], [71], [72], [76]–[78], [83]–[85], [91], [111], [116], [126], [132]. There are other PL models that consider shadowing for NLOS paths, and additional losses incurred from other obstacles [82], [113], [125]. In [113], shadowing loss was considered in the modeling and evaluated as a function of the elevation angle for NLOS paths. The shadowing loss was calculated based on the uniform theory of diffraction. The distribution of the shadowing was found to be normal. Strong shadowing was observed in [125], in an urban area, mostly due to knife edge diffractions from the surrounding buildings. On the other hand, in [82], additional losses were considered at the GS and the UAV for the overall PL modeling.

5) *Modified FSPL Model*: Due to the potential three dimensional motion of UAVs, modified FSPL models accounting for UAV altitude can also be developed; several that are a function of elevation angle are considered

in [108], [112], [114], [126], [133]. In [108], effect of three dimensional antenna radiation pattern is included in the received power calculation. At higher elevation angles with omni-directional antennas at both the TX and the RX sides, the low gain antenna radiation regions in the elevation plane were exposed at the TX and the RX sides resulting in reduction of the received power. This loss, due to small antenna radiation gain in the elevation plane at higher UAV heights was reduced as the UAV moved away from the GS. Similar observations with antenna radiation pattern were made in [126]. In [112], FSPL was provided, taking into account the height of the aerial platform, therefore the distance d obtained from the geometry of the setup in the FSPL expression was modified as $d = \frac{\Delta h}{\sin \theta}$. In [114], PL considering the elevation angle was modeled for $\theta > 10$. The PL was modeled for both LOS and NLOS paths using intrinsic coefficients and claimed to be independent of the antenna heights at the TX and the RX. Similar three dimensional PL model was provided in [133].

6) *Two-Ray PL Model*: The two ray PL model described earlier in Section III-C is provided in [37], [54], [73]–[75], [77]–[79], [91]. In case of two ray PL modeling, the variation of the PL with distance has distinctive peaks due to destructive summation of the dominant and surface-reflected component. In the majority of PL models, PL variation is approximated as a log-normal random variable. This variation can be either due to shadowing from the UAV body (see next subsection) or from MPCs attributable to terrestrial scatterers such as buildings [37], [53], [54], [57], [71], [72], [75], [76], [78], [85], [91], [111], [113].

7) *Log-Distance FI Model*: In [22], log-distance FI models for the PLE and shadowing for the AG radio channel between airborne UAVs and cellular networks are presented for 800 MHz and UAV heights from 1.5 m to 120 m above ground. In [127], the low altitude AG UAV wireless channel has been investigated for a scenario where a UAV was flying above an ensemble of containers at 5.76 GHz. Narrow- and wideband measurements have been carried out. The paper presents a modified PL model and PDPs. Most interesting is that in this particular environment, delay dispersion actually increases with altitude as the UAV rises above metallic structures.

8) *LOS/NLOS Mixture Path Loss Model*: Another common model used in the literature [48], [134]–[139] averages the PL over the probabilities of LOS and NLOS PL as follows [48], [140]:

$$PL_{\text{avg}} = P(\text{LOS}) \times PL_{\text{LOS}} + [1 - P(\text{LOS})] \times PL_{\text{NLOS}}, \quad (5)$$

where PL_{LOS} and PL_{NLOS} are the PL in LOS and NLOS conditions, respectively, $P(\text{LOS})$ denotes the probability of having a LOS link between the UAV and the ground node, given by [48], [140]:

$$P(\text{LOS}) = \prod_{n=0}^m \left[1 - \exp \left(- \frac{[h_U - \frac{(n+1/2)(h_U-h_G)}{m+1}]^2}{2\Omega^2} \right) \right], \quad (6)$$

where we have $m = \text{floor}(r\sqrt{\varsigma\xi} - 1)$, r is the horizontal distance between the UAV and the ground node, h_U and h_G are as shown in Fig. 1 of this survey, ς is the ratio of built-up land area to the total land area, ξ is the mean number of buildings per unit area (in km^2), and Ω characterizes the height (denoted by H) distribution of buildings, which is based on a Rayleigh distribution ($P(H) = (H/\Omega)^2 \exp(-H/2\Omega^2)$). In [48], for a specific value of θ in [48, Fig. 2], a sigmoid function is also fitted to (6) for different environments (urban, suburban, dense urban, and highrise urban) to enable analytical tractability of UAV height optimization. Since (5) averages the PL over large number of potential LOS/NLOS link possibilities, it should be used carefully if used with system-level analysis while calculating end metrics such as throughput and outage. Similarly, PL variability should be added to the model of (5).

Overall, a comparison of different PL models in Table V, shows that two ray PL model is a better choice for open field, rural areas and over sea, whereas higher ray model, e.g., 3 ray or 4 ray model can be employed for environments with larger number of scatterers whose heights are comparable to the height of the UAV. This has been validated by channel measurements carried out in [54], [76], [78], where CE2R model was found to provide better fitting for over water, harbor and mountainous settings, however, the log distance PL model was found to have better fit for the environments with higher scatterers, e.g., urban and suburban. Similarly, two ray PL fitting with L-band was better as compared to C-band. However, in [91], the measured data obtained over sea was compared with FSPL and two ray model, and it was observed that both models overestimated the PL. This was mainly due to ducting effect over sea surface causing reduction in the PL. In [81], the RSS obtained from wideband measurements at 5.06 GHz were found to closely fit the FSPL for one location whereas providing upper bound for another location. However, in [76], with similar propagation environment at C-band, it was observed that CE2R model provided a better fit.

Selection of a suitable PL model for a given AG propagation scenario is pivotal. In most of the literature, the PL model for of (2) is used due to its simplicity and provision of a standard platform based on reference distance FSPL for comparison of measurements in different environments. A reference distance of 1 m is often taken as a standard for short-range systems, but larger values are also used. However, in some scenarios, where the reference FSPL is not available, the FI model (3) may be used. Yet due to lack of any standard physical reference, the FI slope cannot be deemed PLE and will be dependent on the environment. Additionally, the variability of the PL is generally a zero mean Gaussian random variable that has approximately similar values for both the CI and FI model types.

A general recommendation for selection of AG PL model for a given measurement scenario from Table V is as follows: for an open flat or hilly area with light suburban, rural or no terrain cover, and for over water, the two ray PL model or free space reference log-distance model (2) may be preferred. This is due to small number of MPCs reaching the aerial platform and high probability of presence of a dominant LOS and ground reflected component only in these environments.

For complex geometrical environments with large number of scatterers in a LOS path between the GS and the UAV, a DS PL (4) model may be best. This is because the received power can be differentiated into two different categories [108]. One is due to persistent components arising from LOS and ground reflection paths, whereas, others from the surrounding scatterers. Therefore, DS may be a better option for these scenarios. The FI model in (3) may be preferred in certain specialized environments, e.g., [127], due to their ease in applicability and PL model predictions only for a given area. In Table V, the model types denoted log-distance refer to the general log-distance equation for PL with different reference distances and additional parameters.

C. Airframe Shadowing

Airframe shadowing occurs when the body of the aircraft itself obstructs the LOS to the GS. This impairment is somewhat unique to AG communications, and not much exists in the literature on this effect. One reason for this is that such shadowing can be largely (but not always completely) alleviated by using multiple spatially separated antennas: airframe shadowing on one antenna can be made unlikely to occur at the same time as shadowing on the other(s). In addition to frequency and antenna placement, shadowing results also depend on the exact shape, size, and material of the aircraft. For small rotorcraft, depending on frequency and antenna placement, airframe shadowing could be minimal. Example measurement results, as well as models for airframe shadowing, for a fixed wing medium sized aircraft, were provided in [141].

For these results, at frequencies of 970 and 5060 MHz, wing shadowing attenuations were generally proportional to aircraft roll angle, with maximum shadowing depths exceeding 35 dB at both frequencies. Shadowing durations depend upon flight maneuvers, but for long, slow banking turns, can exceed tens of seconds.

An illustration of airframe shadowing is shown in Fig. 6 where received power is plotted against time for a wideband (50 MHz) signal in C-band before, during, and after the medium-sized aircraft made a banking turn. The received power on two aircraft antennas (denoted C1, C2), bottom mounted and separated by approximately 1.2 m, is shown. Attenuations due to airframe shadowing, along with the polarization mismatch that occurs during the aircraft maneuver, exceed approximately 30 dB in this case.

D. Small Scale Fading Models

Small-scale fading models apply to narrow-band channels or to individual MPCs, or *taps* in tapped delay line wide-band models, with bandwidth up to some maximum value (i.e., small scale fading may not pertain to MPCs in a UWB channel). The depth of small scale amplitude fades on a given signal also generally varies inversely with signal bandwidth [142]. Stochastic fading models are obtained through analysis, empirical data, or through geometric analysis and simulations [49]–[51], [64], [111], [119]. As noted in Section VI-A, the GBSCMs can be subdivided

TABLE VI
REVIEW OF THE EXISTING LITERATURE ON SMALL SCALE AG PROPAGATION CHANNEL FADING CHARACTERISTICS

Ref.	Scenario	Time-variant/Time-invariant	Modeling type	Frequency spectrum	Center frequency (GHz)	DS (Hz)	Fading distribution	K-factor (dB)
[68]	Urban/Suburban	Time-invariant	Statistical	Narrow-band	2	-	Ricean	-
[72]	Suburban/Open field	Time-invariant	Statistical	Ultra-wideband	3.1-5.3	-	Nakagami	-
[81]	Suburban/Open field	Time-variant	-	-	5.06	833	-	-
[82]	Urban/Suburban	-	-	Narrow-band	2.3	-	-	-
[57]	Urban/suburban	Time-invariant	Statistical	Wide-band	2	-	Rayleigh, Ricean	-
[71]	Urban/suburban	-	Statistical	Wide-band	5.75	1400	Ricean	(-5)-10
[78]	Urban/Suburban	Time-variant	Statistical	Wide-band	0.968, 5.06	-	Ricean	12-27.4 in L and C band
[92]	Hilly	Time-variant	-	Wide-band	5.12	5000	-	-
[86]	Forest/foliage	-	Statistical	Ultra-wideband	8-18	-	Ricean, Nakagami	2-5
[77]	Sea/fresh water	Time-variant	Statistical	Wide-band	0.968, 5.06	-	Ricean	12, 28 for L and C band
[67]	-	Time-variant	Statistical	Wide-band	5.135	5820	-	-

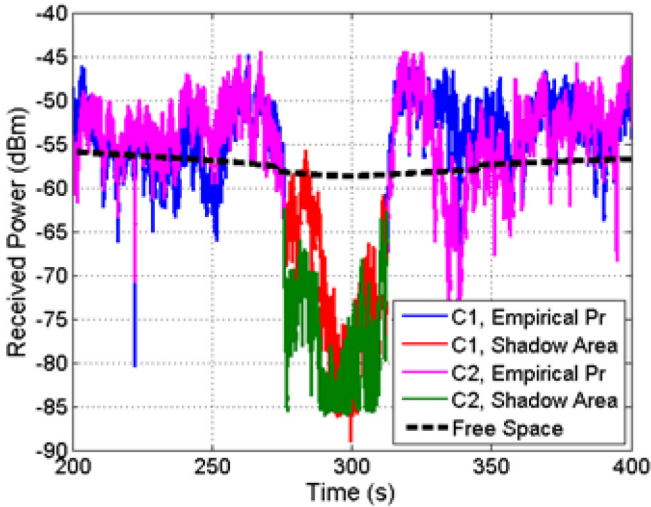


Fig. 6. Received power vs. time for illustration of shadowing before, during and after the banking turn of medium sized aircraft at C-band.

into RS-GBSCM and IS-GBSCM. In [119], a time-variant IS-GBSCM was provided with a Ricean distribution for small scale fading. Time-variant RS-GBSCM were provided in [50], [64], and these also illustrated Ricean small scale fading.

A NGSCM was provided in [66], where GA fading was described using Ricean and Loo models. The Loo model was derived based on the assumption that the amplitude attenuation of the LOS component due to foliage in a land mobile satellite link follows a log-normal distribution, and that the fading due to MPCs follows a Rayleigh distribution. The switching between Ricean and Loo models was controlled by a Markov process dependent on flight height. In [51], a GBSCM for MPCs was provided in the form of shape factors describing angular spread, angular compression, and direction of maximum fading using the probability density function (PDF) of angle of arrival.

Table VI provides measured small scale AG fading characteristics reported in the literature for various environments. As previously noted, the most common small scale fading distribution for AG propagation is the Ricean. As in terrestrial channels, for the NLOS case, the Rayleigh fading

distribution typically provides a better fit [57], [65], [68], [69], [71], [120], [143], and of course, other distributions such as the Nakagami-m and Weibull distributions might also be employed. Small scale fading rates depend upon velocity, and these rates are proportional to the Doppler spreads of the MPCs [70], [71], [74], [81].

E. Intermittent MPCs

Another AG characteristic that may be of interest in high-fidelity and long-term channel models is the intermittent nature of MPCs. From geometry, it is easy to deduce that for a given vehicle trajectory in some environment, individual MPCs will persist only for some finite span of time [54]. This has been noted in V2V channels as well, but with UAVs and their potentially larger velocities, the intermittent MPC (IMPC) dynamics can be greater. These IMPCs arise (are “born”) and disappear (“die”) naturally in GBSCMs. They may also be modeled using discrete time Markov chains. The IMPCs can significantly change the CIR for some short time span, hence yielding wide variation in RMS-DS. (Another manifestation of so-called “non-stationarity.”) Example models for the IMPCs—their probability of occurrence, duration, delay, and amplitude—appear in [54], [58], [79], [108]. In these studies it was found that IMPCs follow a random process which is highly dependent on the geometry, and distribution of the scatterers around a given UAV trajectory.

In Fig. 7, from [37] the fading of MPCs as a function of time and delay are shown. The amplitude of MPCs generally decay with excess delay at a given time instant. Additionally, there is a continuous birth and death process of MPCs at different instants of time. This can be represented using CIR as [37]:

$$h(t, \tau) = \sum_{i=0}^{M(t)-1} p_i(t) a_i(t) \exp(j\phi_i(t)) \delta(\tau - \tau_i(t)), \quad (7)$$

where $h(t, \tau)$ is the time variant CIR, $M(t)$ is the total number of MPCs at time instant t , $p_i(t)$ represents the multipath persistence process coefficient and can take binary values [0, 1]. The amplitude, phase and delay of i^{th} MPC at time instant t are represented as $a_i(t)$, $\phi_i(t)$ and $\tau_i(t)$, respectively. The phase term is given as $\phi_i(t) = 2\pi f_d^i(t)(t - \tau_i(t)) - f_c(t)\tau_i(t)$, where $f_d^i(t) =$

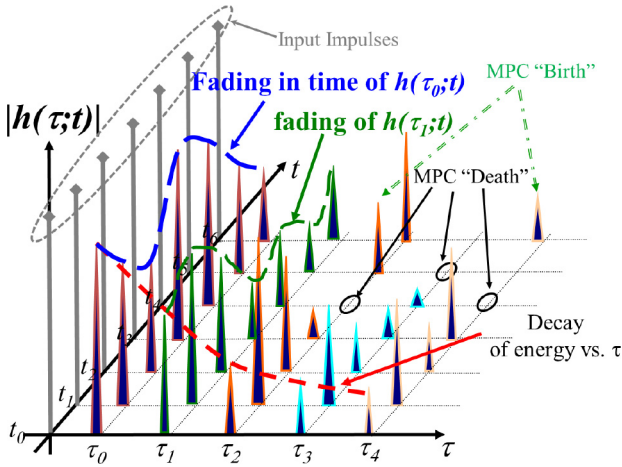


Fig. 7. Fading and birth and death process of intermittent MPCs from [37].

$v(t)f_c(t)\cos(\Theta_i(t))/c$ is the Doppler frequency of the i^{th} MPC, $\Theta_i(t)$ is the aggregate phase angle in the i^{th} delay bin, c is the speed of light and f_c represents the carrier frequency. The channel transfer function $H(f, t)$ from (7) is then given as follows:

$$H(f, t) = \sum_{i=0}^{M(t)-1} p_i(t) a_i(t) \exp(j2\pi f_d^i(t)(t - \tau_i(t))) \times \exp(-j2\pi f_c \tau_i(t)) \exp(-j2\pi f \tau_i(t)), \quad (8)$$

The effect of the Doppler spread is typically negligible compared to carrier frequency at lower velocities. Therefore the carrier frequency term will dominate the variation of the transfer function.

Fig. 8(a) shows a sequence of PDPs versus link distance for a near-urban AG link near Cleveland, OH, USA. Flight parameters can be found in [78]. In this figure, the IMPCs are clearly visible, here caused by reflections from obstacles near the Lake Erie shoreline. In Fig. 8(b) RMS-DS vs. link distance for a hilly environment in Palmdale, California is shown. The intermittent nature of the MPCs produces “spikes” and “bumps” in the RMS-DS values, illustrating the potential rapid time variation of AG channels.

F. Effect of Frequency Bands on Channel Models

The selection of frequency bands for CNPC and payload communications using AG links for UAVs are discussed in Section III-B. In the literature, most of the AG propagation channel measurements were carried out using wideband spectrum, whereas some narrowband channel measurements are also available. The current and future communications are expected to deploy OFDM technology. Therefore, narrowband employed by OFDM needs to be studied extensively in different AG propagation environments. The propagation channel characteristics using narrowband are expected to be affected more as compared to wideband in case of UAV in motion especially in a scatterer rich environment, e.g., dense suburban. This is due to fading, affecting the narrowband more as compared to the wideband when the UAV is in motion.

UWB AG propagation channel measurements in the frequency band 3.1 GHz - 5.3 GHz were performed in open

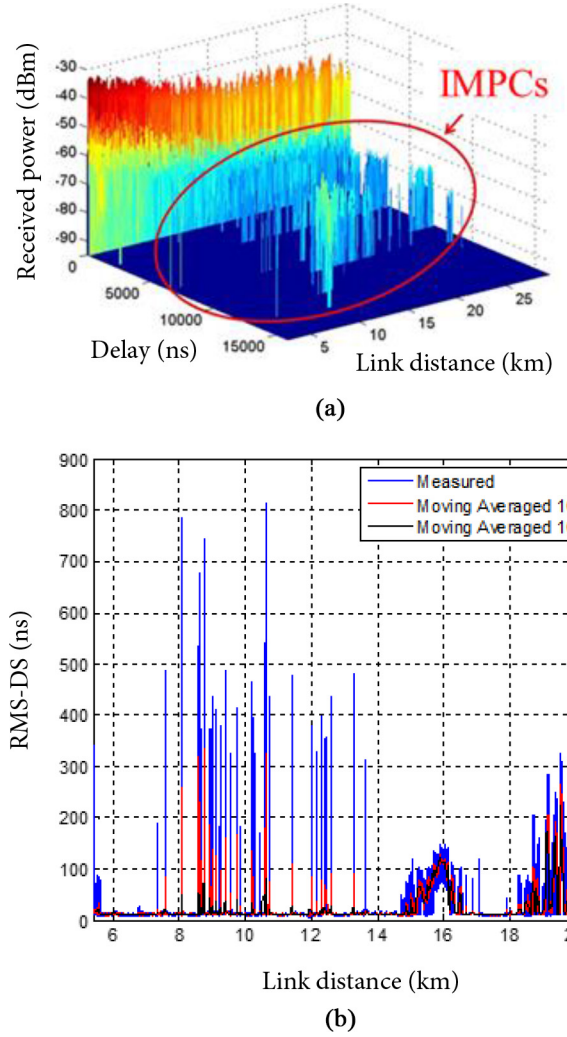


Fig. 8. (a) Sequence of PDPs versus link distance for a near-urban AG link near Cleveland, OH, USA. (b) RMS-DS vs. link distance for a hilly environment in Palmdale, California.

and suburban areas in [72]. A narrow sub-band frequency analysis was provided, where higher mean attenuation and larger variance of received power was observed at higher frequency sub-bands. Narrowband frequency measurement campaign for three different frequencies of 2 GHz, 3.5 GHz, and 5.5 GHz was carried out in an urban area in [113]. Higher attenuation was observed at respective higher frequency bands, whereas the standard deviation did not show much difference for three different frequency bands. Wideband channel measurements at L-band and C-band were provided in [54], [76], [78] for different propagation environments. Different attenuation, and small scale effects were observed at the two different frequency bands in a given propagation environment, e.g., in [76], channel measurements were performed in a hilly/mountainous area. Similarly, higher K -factor and PLE were observed for C-band as compared to L-band, whereas, larger shadowing variable was reported for L-band as compared to C-band.

The mmWave AG propagation channel characteristics using UAVs at 28 GHz and 60 GHz in different environments were provided in [93] using ray tracing simulations. The RSS generally followed a two ray model at both frequencies in

different propagation environments, however, higher rate of maxima/minima at 60 GHz was observed as compared to 28 GHz. In [82], two ray model was used for PL representation at 2 GHz in an urban environment, whereas, channel measurements at 2 GHz obtained in [57] in a similar environment were found to be better fitted with a log distance PL model.

G. MIMO AG Propagation Channel Models

The use of MIMO systems for AG UAV communications has been gaining popularity. The rationale, increased throughput and reliability, is the same one driving mmWave and future 5G research. In [144], it was shown that it is possible to attain higher spatial multiplexing gains in LOS channels by properly selecting the antenna separation and orientation as a function of carrier wavelength and link distance. This careful alignment is not always practical or possible with UAVs, especially when mobile.

The advantages of spatial diversity and multiplexing gains in MIMO are often only moderate due to limited scattering available near UAVs or GSs. In [145], it was demonstrated that due to limited spatial diversity in the AG channel, only moderate capacity gains are possible. In order to obtain better spatial multiplexing gains, larger antenna separations are required, and this requires large antenna arrays that are not feasible on-board small UAVs. Use of higher carrier frequencies makes it possible to use electrically-large antenna arrays, but higher frequencies yield higher PL (this can be mitigated somewhat by beamforming, at the expense of the complexity required for beam steering). Moreover, accurate channel state information (CSI) is important for MIMO systems for higher performance, but in a rapidly varying AG propagation channel, it can be difficult to provide accurate CSI and hence MIMO gains can be limited. The use of MIMO on airborne platforms also incurs additional cost, computational complexity, and power consumption.

There is a limited number of studies available in the literature for MIMO AG propagation channel measurements. In [62], a detailed measurement analysis of the AG MIMO propagation channel was provided. It was observed that a considerable spatial de-correlation of the received signal at the GS is achieved due to the interaction of non-planar wavefronts. These wavefronts are generated due to near field effects from the measurement vehicle, on which the GS antennas were mounted. Spatial diversity from antennas located on the UAV was also observed, interestingly at *higher* elevation angles. The authors suggest that having scatterers near the GS can yield larger spatial diversity. The received signal in [87] was analyzed for multiple-input-single-output (MISO) and MIMO systems, and it was observed that the use of MIMO systems enables a more robust channel for changes in antenna orientations arising from UAV maneuvering. In [89], MIMO system performance was tested in different scenarios of the outdoor environment, including urban, rural, open field, and forest. The effect of terrain cover on the received power was analyzed for these different scenarios with the result that the propagation channel in the open field is mostly influenced by the ground

reflections, whereas in case of forests, the reflection and shadowing from the trees is a major contributor to the propagation channel characteristics. In rural and urban cases, the reflections from the walls and surfaces of building structures play an important role.

Time-variant GBSCMs for MIMO systems provided in [50], [64], [119], [146] were explored through simulations. Where, different propagation geometries and scatterer distributions were used in order to analyze the capacity for MIMO AG channels. A common observation was that higher capacity is achievable with MIMO AG systems. A simulation based AG MIMO channel propagation model was provided in [111] for a hilly area. The results indicate increased throughput from spatial multiplexing and higher SNR from the MIMO system in comparison to SISO, as expected. A stochastic model for a mobile to mobile AG MIMO propagation channel was presented in [50]. These results show that there was considerable capacity increase and reduction in outage probabilities using MIMO systems if perfect instantaneous CSI is available. In [146], geometry-based simulations were conducted for a massive MIMO implementation for a UAV AG propagation channel. The simulation results illustrate the expected result of a significant capacity increase when a large number of antennas is used at the GS.

H. Analysis and Comparison of Different AG Propagation Channel Models

In this subsection, we will briefly analyze and compare different AG propagation channel models for UAVs in the literature.

1) Large Scale Fading Models: Large scale fading models for AG propagation available in the literature, generally can be fitted with a modified FSPL model. In [72], PL was measured for open and suburban scenarios in the presence and absence of foliage. The PL was found to be highest for the foliage due to obstruction. In addition, the PL was found to be dependent on the height of the GS, apart from the height of the UAV. The PLE reported was above 2.5 for all the propagation scenarios involving open and suburban areas. Additionally, the PLE for suburban scenario was slightly higher than the open area scenario. In [86], PL due to diffraction and scattering from different species and parts of the tree are provided. It was observed that loss from the trunk of the tree is due to diffuse scattering, whereas, it was mostly due to diffraction on the edges of the crown of the tree. In [53], [54], [58], [75], [76], [78], PL for channel measurements in the urban, suburban, hilly, mountainous, and over sea scenarios were provided. A comparison of PL obtained from free space, analytical CE2R model and measurements was provided. The PLE for C-band and L-band for different measurement scenarios was found to be approximately equal or less than the FSPL. For over sea scenario, ducting was not observed whereas in [91], ducting was observed that resulted in reduction of the PL as compared to the FSPL. A study for PL during different flight scenarios of take off, en-route, landing, taxiing and parking were provided in [71]. Higher PLE was observed for take off and en-route as compared to other flight scenarios. In [125], excess PL was provided for an urban scenario. It was found that excess loss

was dependent on different diffractions from the edges of the surrounding buildings.

Antenna orientation effects on the RSS were provided in [61], where the PLE was found to be close to FSPL in different antenna orientations in urban and open field. The PLE was found to be higher in the urban area as compared to open field. A similar study taking into account the antenna radiation effects is available in [108], [126], where it was found that minimum received power was observed when the UAV was on the top of the base station due to minimum antenna gain in the elevation plane at that point.

2) Small Scale Fading Models: In the literature, there are limited small scale models for AG propagation using UAVs. However, there is a comprehensive wideband measurement and modeling campaign at the L-band and C-band available in the literature [54], [76], [78]. This campaign was conducted in different propagation environments over sea, hilly, mountainous, suburban and urban areas. This campaign provides the bulk of the small scale modeling information for AG propagation channels in the L-band and C-band. A TDL model was used to represent the channel response in all the scenarios. A two ray model in addition to varying number of intermittent MPCs in different environments. K -factor obtained from measurements provided a measure of the strength of MPCs when compared with the LOS component. In all the scenarios, the K -factor for C-band was found to be higher than the L-band. The highest K -factor was observed for the C-band for the over sea scenario, followed by hilly/mountainous, and suburban/urban scenarios. The K -factor in the L-band was found to vary less in different propagation environments as compared to the C-band.

A small scale propagation channel model for UWB was provided in [72], for suburban and open field scenarios. The small scale fading amplitudes were found to be Nakagami distributed. A modified Saleh-Valenzuela model was used to model the CIR. Different number of MPC clusters were observed in the open field as compared to the suburban environment. It was observed that the RMS-DS changed with the height of the UAV in the suburban scenario, whereas it was approximately flat for the open field scenario. Similarly, higher TOA of MPCs was observed for suburban scenario as compared to open field for different UAV heights. In [68], second order channel statistics of average fade duration and level crossing rate were provided for the narrowband AG signal propagation. The amplitude of the MPCs was found to be log-normally distributed. A time series generator was used for emulation of RSS based on the analytical model and compared with the measurement results.

I. Comparison of Traditional Channel Models With UAV AG Propagation Channel Models

The UAV AG propagation channel naturally has similarities with outdoor terrestrial propagation channels, at least for elevated base stations. We do not provide a comprehensive comparison between UAV AG channels and terrestrial channels here, as there are numerous terrestrial channel models for a variety of terrestrial environments [147] that differ based

on specific environment, center frequency of operation, bandwidth, antenna type and configuration, among other factors. Here we provide some remarks for context.

Among other applications, UAVs are likely to be used in future cellular communication networks either as a base station [148], [149] or a user equipment node [83]. When a UAV is used as a base station, the corresponding propagation channel *may* exhibit cellular base station characteristics if they are hovering (with no mobility) at similar heights/environments as in terrestrial base stations, and assuming they communicate with similar user equipment as in terrestrial cellular networks. In such cases, terrestrial cellular channel models might be applicable for AG channels [147].

On the other hand, many times the UAVs may be mobile, might operate at significantly higher altitudes than terrestrial base stations, and the operational environment may also be very different, all of which should be taken into account for the channel model. A major difference in the AG channel would be that for typical situations, the vast majority of scatterers are located around the GS and not the UAV. This of course has a direct influence on the MPC characteristics, mainly the Doppler frequencies of the MPCs. In particular, if the UAV is moving and while the GS is stationary, all MPCs usually have a very similar Doppler frequency, in strong contrast to the terrestrial channel.

When the UAV is used as a user equipment node (communicating with a terrestrial base station), the terrestrial cellular channel models cannot be directly applied [107]. This is true because when aloft, hovering or moving, the UAV experiences large and small scale fading characteristics different from ground based users because of the different spatial distribution of nearby obstacles. Channel models for a user equipment node as a UAV in a cellular communication network are provided in the recent version of the 3GPP documentation covering UAV communications [150]. Details are discussed in Section VI-K.

One can also compare UAV channel models with satellite channel models [151], [152]. Overall, both satellite and UAV communication links have higher probability of LOS than terrestrial cellular links [153]. One of the main differences is that for most satellite applications, we are not interested in small elevation angles (e.g., smaller than 5°). This is due to the negative effects of the tropo-/ionosphere on the propagation. However, in the AG channel we often end up with very low elevation angles and long link distances: this implies that the effects of the troposphere can be significantly larger than for the typically high elevation angles used in satellite applications. Many satellite communication links are directional and point to point, whereas UAV communications need not be directional.

J. Ray Tracing Simulations

In the literature, in addition to measurements, channel characterization for AG propagation is also carried out using simulations. These simulators are either based on customized channel environments on a given software platform or can be realized using ray tracing simulations. There are PL models available for these simulated environments [48], [112],

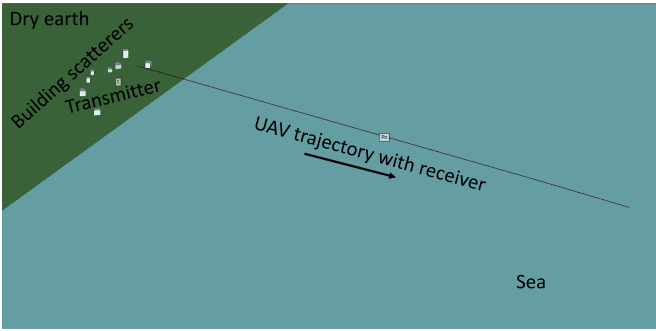


Fig. 9. Ray tracing simulation scenario for over sea scenario, where the UAV flies over a straight line.

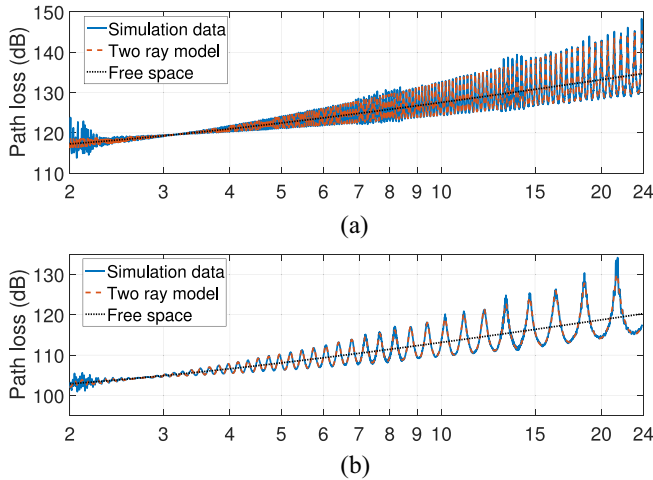


Fig. 10. Ray tracing PL results for over sea water settings, (a) C-band (5.03 GHz - 5.091 GHz), (b) L-band (0.9 GHz - 1.2 GHz).

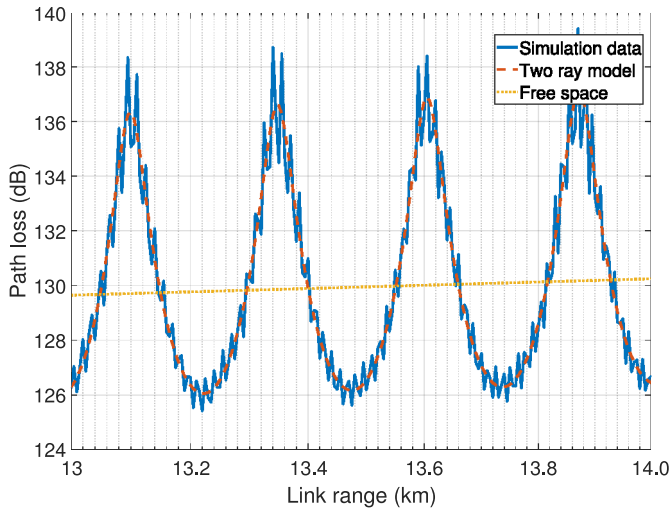


Fig. 11. Zoomed in results of PL for over sea water simulations of Fig. 10 for C-band at link distances of 13 km - 14 km.

[114], [116], [133], [143]. Urban environmental scenarios for LOS and NLOS paths were considered in [48], [112], [114] where log-distance and modified FSPL models were suggested. In [116] a log-distance path model was provided for LOS and NLOS paths for over sea settings in a simulated environment. However, to the best knowledge of the authors,

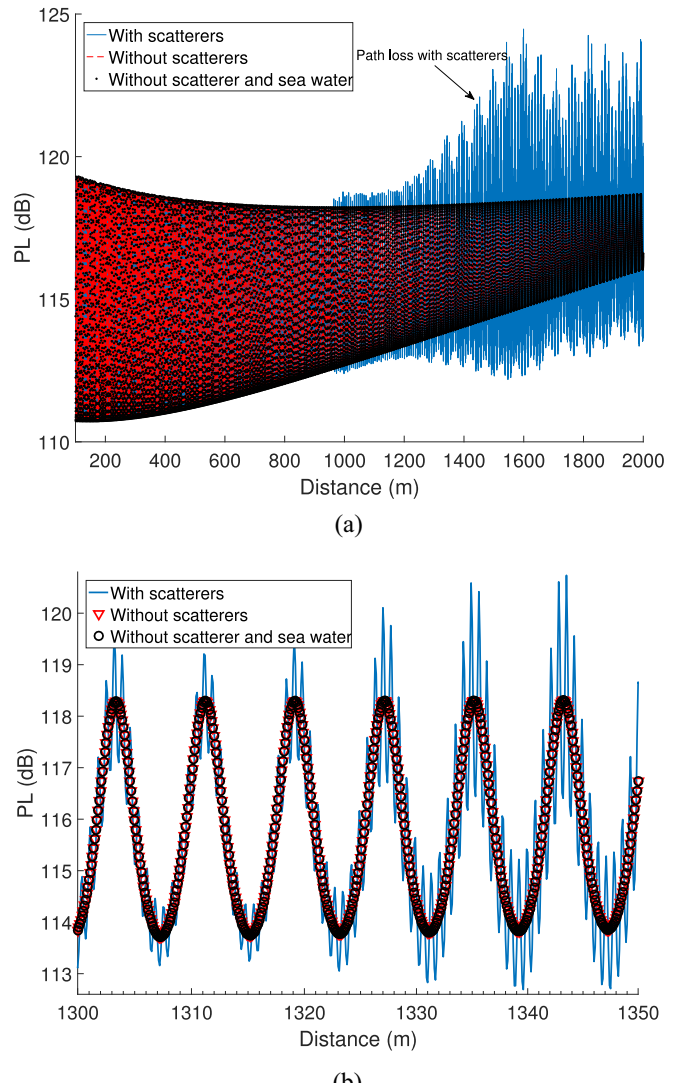


Fig. 12. Path loss versus distance with/without scatterers, and without the sea surface: (a) 100 m to 2 km range, and (b) 1300 m to 1350 m range.

there are no specific experimental studies available in the literature that experimentally validate the channel models proposed using geometrical analysis and simulations in [48], [112], [114], [116], [133], [143].

Ray tracing was used for mmWave channel characterization for 28 GHz and 60 GHz frequency bands for UAV AG propagation in [93]. Different environments were realized, namely urban, suburban, rural and over sea. It was observed that the RSS followed the two ray model and is further affected by the presence of scatterers in the surroundings. The RMS-DS was also affected by the presence of scatterers in the surrounding environment and the UAV height in the given environment. If the height of the scatterers were comparable with the UAV height, higher RMS-DS was observed due to multiple reflections from the randomly distributed scatterers. In contrast, if the height of the scatterers is small, we have smaller RMS-DS at higher UAV heights due to fewer significant MPCs reaching the UAV. This phenomena is verified at 28 GHz and 60 GHz, where at 60 GHz, we have smaller RMS-DS than at 28 GHz due to higher attenuation of MPCs.

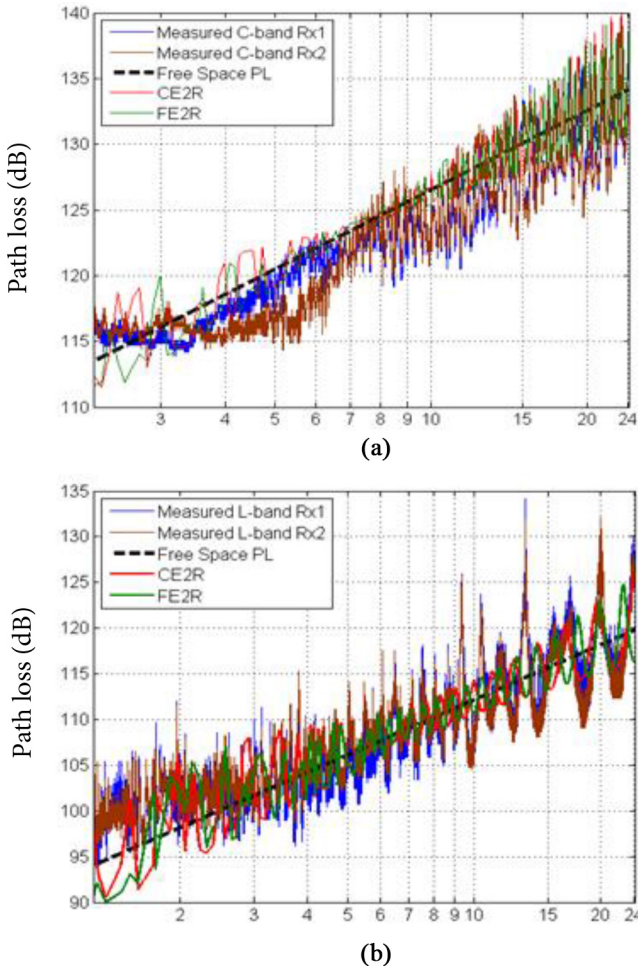


Fig. 13. Measurement results for PL over sea scenario from [54]: (a) C-band (5.03 GHz - 5.091 GHz), (b) L-band (0.9 GHz - 1.2 GHz).

Ray tracing simulations using Wireless InSite software were carried out to estimate PL for an over-sea scenario as shown in Fig. 9. The channel measurement parameters were set according to [54], and the simulated PL results were compared with the measured values. Fig. 10 shows the simulated PL results. In this simulated environment, we have buildings as scatterers near the TX. Due to reflections and diffractions from these scatterers we observe additional fluctuations on top of the two ray propagation model. The deviations are due to MPCs reflected and diffracted from the different-shaped scatterers at different angles. These weak MPCs reach the UAV RX at different link distances resulting in variations from the two ray model as shown in Fig. 11 at a link distance between 13 km - 14 km.

Similarly in Fig. 12(a), the effect of MPCs from scatterers around the TX for link distances 100 m - 2 km are shown. It can be observed that without the scatterers and seawater (with ground only), we have a perfect two ray PL model. Yet in the presence of the scatterers around the TX, superimposed upon this effect is variation from additional MPCs from the scatterers; this yields what can be modeled as a random PL component on top of the two ray model, or in effect a small scale fading. This effect is of course dependent on

the geometry of the scenario and will cause the PL to vary along the trajectory of the UAV. A similar effect at the larger link distance range of 13 km - 13.5 km in Fig. 12(a) can be observed in Fig. 12(b).

Fig. 13 shows measured and model PL results from [54] for over-sea settings. There is a good match between the ray tracing simulation results and analytical results for this over sea scenario in Fig. 10, but when comparing measurement data with simulation data, we observe more fluctuations in measurements due to several factors: measurement equipment variation, ambient noise, and in particular scattering from the rough sea surface, which is not as easily modeled with the basic ray tracing. Also, plotted along with the measurement data in Fig. 13 are analytical results for free space and curved- and flat-earth two ray models. The curved- and flat-earth two-ray models are obtained using the specific geometry and conditions of the measurement environment.

K. Channel Models for 3GPP Cellular-Connected UAVs

The latest version of 3GPP model [150] provides channel modeling details for UAV AG communications, considering the user equipment on the UAV communicating with the fixed base station. These details include LOS probability, PL models, and fast fading models. The height of the user equipment on-board UAV in the air can be smaller or greater than the base station height.

LOS probability for rural macro (RMa), urban macro (UMa), and urban micro (UMi) are provided for different aerial user heights. The LOS probability is smaller for all the scenarios when the UAV height is small due to obstruction from scatterers on the ground. As the height of the aerial user increases, the LOS probability also increases, e.g., for RMa scenario, we have 100% LOS probability after 50 m of aerial user height, whereas it is 100 m for UMa scenario. The LOS probability expression is dependent on the height of the UAV. For example, for a RMa scenario, with a UAV height in the range of 10 m - 40 m, and for a UMa and UMi scenario with a UAV height range of 22.5 m - 100 m, the LOS probability expression is given as follows [150]:

$$P_{\text{LOS}} = \begin{cases} 1, & \text{for } (d_h \leq d_1) \\ \frac{d_1}{d_h} + \exp\left(-\frac{d_h}{p_1}\right)\left(1 - \frac{d_1}{d_h}\right), & \text{for } (d_h > d_1) \end{cases} \quad (9)$$

where d_h is the horizontal distance of the UAV from the base station. The value of variables d_1 and p_1 are dependent on the UAV height and the scenario considered.

The PL models are modified FSPL models taking into account the height of the user with respective constants. For the three scenario of RMa, UMa, and UMi, the lower bound height of user is 1.5 m and goes up to 300 m. The PL models using UAVs are divided into two categories based on the height of the aerial user. For a RMa scenario, with height of aerial user in the range 1.5 m - 10 m, PL model from [154, Sec. 7.4] were recommended for both LOS and NLOS paths, whereas for aerial user heights of above 10 m, additional PL models are provided for LOS and NLOS paths [150]. Similarly, for the UMa and UMi scenarios, instead of 10 m, 22.5 m

upper bound height is used for separation of two PL model categories. The distribution of the shadow fading in all the scenarios is found to be log-normal. The standard deviation of the shadow fading for LOS scenarios for aerial user height of above 10 m for RMa and 22.5 m for UMa and UMi is a function of height of the aerial user. On the other hand, for aerial user height of less than 10 m for RMa, and 22.5 m for UMa and UMi, and NLOS scenarios it is assigned a constant value.

Fast fading models are also provided in [150] for aerial users. The models are provided for aerial user height of 10 m - 300 m for RMa and 22.5 m - 300 m for UMa and UMi. Three different alternatives are provided for evaluation of fast fading models. In each alternative specific parameters are provided or parameters from [154] are used for fast fading modeling for RMa, UMa, and UMi scenarios.

VII. FUTURE RESEARCH AREAS FOR AG UAV CHANNEL MEASUREMENTS AND MODELS

In this section we discuss limitations of currently available AG channel measurements and models and their possible enhancements. We also identify some representative considerations for future research. Our aim is to incite development of more comprehensive, realistic, and accurate propagation channel models for future UAV communication applications.

A. Future Small UAV Scenarios

In future scenarios small UAVs will fly in cities, across suburban areas, and over rural terrain. There are two conceptually very different communication approaches for small UAVs: the first approach is based on centralized communications, i.e., UAVs communicate with base stations similar to the concept of 3G and 4G cellular mobile radio. These base stations would preferably be located on elevated positions such as towers or roof tops and have antennas whose radiation patterns are optimized for serving these UAVs. The second approach foresees direct communications among all UAVs, similar to vehicular communications such as ITS-G5 (intelligent transportation systems communications standard at 5.9 GHz). Both approaches have their pros and cons in terms of robustness, latency, and capacity; as implied, no decision has been made so far on which approach to use and only a few channel measurements have been carried out so far for both approaches.

The scenarios that have to be considered for future propagation measurements should encompass urban, suburban, industrial, rural, and even indoor or “quasi-confined” areas such as large arenas or stadiums. Attention should be directed not only to en-route situations; even though these might be less demanding in terms of propagation conditions, strong MPCs are likely to occur due to reflections from smooth wet ground or bodies of water, and from large buildings with metallized window fronts. In addition we also recommend investigating the channel for take-off and landing scenarios, be it on roof tops, in gardens, or in other specifically assigned areas. In these take-off and landing conditions, propagation may be unfavorable due to shadowing, strong diffraction, and

rich multipath, and it is in these cases where communication must work very reliably. Moreover, we think that the propagation conditions for flights that bring UAVs intentionally close to building facades, power lines, containers, and other objects (e.g., for inspection) should also be investigated as such propagation may exhibit special or atypical features.

In addition of using UAVs as a node in different propagation environments for data source and relaying, they can be employed for data ferrying operations, similar to aerial communication postal service. A possible scenario can be sending data to a remote location not accessible through a direct radio link. This task would be accomplished by first loading data onto a UAV and then taking it to the desired location for transmission.

1) *Cognitive Communications Using UAVs:* The CNPC links for UAVs are critical for safe operation of the UAVs. However, only specific frequency bands are suited for these links. With the introduction of new communication devices into the already congested unlicensed bands, it is imperative to find alternate frequency bands that are robust and reliable for CNPC links. Cognitive radio technology (CRT) can offer a possible solution to this problem [155]–[157]. In these studies, advantages of using CRT technology with UAVs are discussed, e.g., dynamic spectrum access, reduced energy consumption and smaller delays as compared to current UAV communication approaches. Similarly, future applications of using CRT with UAVs are discussed in the field of traffic and border surveillance, disaster relief operations and military applications in the battlefield. Some of the future challenges include design of antenna and specific medium access, routing and transport layer protocols that are optimally efficient during mobility. Overall, CRT can help in accessing licensed and unlicensed frequency bands for robust operations of telemetry in different propagation environments. In addition, CRT can be used for different payload AG communications. However, a major hurdle in implementing the CRT technology for CNPC operations is the safety of flight operations due to dynamic spectrum access.

2) *Artificial Intelligence Integration Into UAVs:* Artificial intelligence (AI) is expected to affect every aspect of our future lives. Integration of AI into self driving vehicles is now a reality [158], [159]. Similarly, many autonomous flying operations are integrated into UAVs, e.g., autopilot, collision avoidance. However, integrating a wider spectrum of AI into UAVs for different future applications can result in revolutionized performance. These integrations in the communication domain on-board UAVs include optimum three dimensional path planning, frequency selection for CNPC operations for different propagation environments, beam steering, and data load balancing. However, higher standards of safety are required for the autonomous working of UAVs.

3) *Marine Applications:* Apart from exciting future applications on the ground, UAVs can be used for different future marine applications. These applications include monitoring of the sea surfaces using radar, using sonar to study underwater marine life and seabed characteristics, surveying of ship passage lanes in constantly shifting ice sheets around the poles.

Similar to sea based applications, UAVs can be used for different fresh water applications, e.g., monitoring the water flows at different points on a river or barrage. The real time data collected using sensors on-board UAVs can be sent to remote monitoring stations either through satellite or radio links.

B. UAV AG Propagation Measurements

Existing AG propagation channel measurements and models mostly apply to aeronautical communications at higher flight altitudes than envisioned for small UAVs. These smaller structures have limited on-board computation capabilities, strict power limitations, and can only fly at much lower altitudes, and at present, only for short durations. There is a growing demand for higher data rates, low latency, and high reliability for future communications, and this will be challenging for current civilian UAV architectures.

Additionally, as noted in Section I, there are usually two types of communications maintained simultaneously for UAVs: payload and CNPC. However, currently there are no standards adopted worldwide for these two types of communications for UAVs. Both can have their own operating bands that may or may not overlap. The CNPC communication links are pivotal for maintaining safety of flight and any interference can be catastrophic. Standards organizations are thus working on robust *loss of link* procedures. Moreover, the CNPC needs to be secure and resistant to jamming and hacking attacks. The USA has developed a standard, primarily for medium and large aircraft [160], with standards envisioned for smaller UAVs in the future.

Future measurement campaigns should take into account not only a great variety of buildings - small and large ones, rectangular and irregularly shaped ones, industrial facilities, halls, and towers - but also reflecting areas like bodies of water, streets, and squares, and demanding situations when a UAV lands on a terrace or the like. Especially for modeling the UAV-to-UAV channel, different velocities and flight situations should be investigated, e.g., two UAVs flying toward each other, with one UAV near ground and the other up in the air, and swarms of UAVs flying with the same velocity. For cellular-like deployments, interference is likely to be a significant issue that influences network planning. Thus, it would be useful to have measurements up to far distances (and over different terrain). We envisage that the UAV-to-UAV channel for small UAVs in urban areas is as diverse as the car-to-car channel, the latter being modeled as a 2.5 dimensional channel whereas the UAV-to-UAV channel will often need to be modeled as a 3 dimensional channel.

UAV Communications are likely to operate in protected frequency bands. The frequency assignments can be exclusive or on a primary basis, but these regulations may not prevent interfering signals which can drastically degrade the performance of the UAV communication system. Interfering signals are unintentional or intentional. Both cases have to be considered although the first case might be more frequent. We recommend assessing the expected amount of interference and measuring interference in various environments. The focus should be on highly populated as well as industrial areas

which are known to exhibit interference in various frequency bands. For the development of countermeasures the relevant parameters of the interfering signals shall be assessed such as typical locations of interfering TXs, transmit power, antenna patterns, bandwidth, duty cycle, and optionally modulation schemes.

In addition to the UAV settings, there are several other factors that need to be taken into account for comprehensive AG propagation measurements using UAVs. One of these is the placement and orientation of antennas. The placement of antennas should be such that there is minimum shadowing and noise effect from the air-frame and motors while flying. Achieving this is not always easy, and will usually be UAV-specific. The antenna orientation has been shown to result in different throughputs and RSS values [60], [61], [84], [85] for different flight maneuvers. In order to provide better coverage during flight, omni-directional antennas on both the TX and the RX are commonly used, especially for CNPC communications. An important factor during UAV flight with omni-directional antennas is the three dimensional pattern of the antenna radiation [108]. This factor is important when the elevation angle between the GS and the UAV is high. Use of directional antennas is dependent on the specific application and coverage. When selecting UAV antenna options, the mechanical viability for a given UAV type should also be taken into account, e.g., a long helical antenna or yagi uda structure may be difficult to mount on a fixed wing aircraft compared to a horn or patch antenna.

There is no fixed number of antennas recommended for optimum performance, and the number of antennas will depend on the operating frequency, UAV size, and operational environments. In many experiments multiple antennas are used on UAVs, and these may be helpful for improved coverage and diversity gains, but at the expense of increased computation, space, and power requirements.

The ambient conditions on-board UAVs must also be taken into account for precise measurement of any communication link characteristics (for CNPC or otherwise). These ambient conditions include noise from the motors, noise from aircraft electronics, air friction while moving, sudden air gusts, temperature variations, and outside-system interference. The latter may be particularly severe for unlicensed bands. Another consideration with the use of unlicensed bands and commodity radios is that the adaptive modulation and coding algorithms employed for terrestrial networks (which often assume quasi-stationary conditions) may not work so well when directly applied to highly dynamic UAV AG propagation channels.

Nearly all current day channel measurements take advantage of positioning information, typically from global navigation satellite systems, with GPS being the most widely used. In addition to position information, GPS signals also provide an accurate time reference. Depending on measurement requirements and the envisioned application, the accuracy of GPS may or may not be sufficient, and this should be considered before beginning measurement campaigns.

When using UAVs in swarms, the location and mobility aware routing methods that are used for terrestrial networks may need to be adapted to account for the three dimensional

movement of UAVs. Similarly, route selection algorithms for mobility aware networks will need to consider the fast varying channel conditions during UAV flight.

C. UAV AG Propagation Channel Models

The UAV AG propagation literature mostly covers the modeling of PL, as described in Section VI-B. As noted, and as is common for terrestrial channels, the PL models are typically provided as a function of link distance. For UAVs there might be other models appropriate for certain cases, for example a PL model as a function of UAV altitude in a given setting, or even indoor UAV PL models for certain settings (e.g., large arenas).

The most accurate UAV AG propagation channel models are of course time varying, but in some cases these can be specialized to time-invariant approximations, e.g., when a UAV is hovering above an area of static objects. In [54], [58], [76], [79], the channel is considered to be quasi stationary only for short distances, and small scale fading parameters are evaluated over that stationarity interval. Additional studies of the stationarity distance should be conducted for other UAV propagation scenarios, using multiple metrics: the PDP correlation coefficient, correlation matrix collinearity, spectral divergence, and evolutionary spectrum have all been used, but each metric has its own advantages and disadvantages. Depending on environments, additional UAV measurement campaigns will likely result in more elaborate UAV AG propagation channel models, that may make use of MPC clusters, spatial (angular) information, and correlations among model parameters. Ultimately, deterministic and hybrid channel models using GBSCM principles will likely evolve to be the most widely used to characterize UAV AG propagation.

VIII. CONCLUDING REMARKS

In this paper, we have provided a comprehensive survey for AG propagation channels for UAVs. The measurement campaigns in the literature for AG propagation were summarized, with information provided on the type of channel sounding signal, its center frequency, bandwidth, transmit power, UAV speed, height of UAV and GS, link distance, elevation angle, and local GS environment characteristics. Air-ground channel statistics from the literature were also provided. Various UAV propagation scenarios and important implementation factors for these measurements were also discussed. Large scale fading, small scale fading, MIMO channel characteristics and models, and channel simulations were all described. Finally, future research directions and challenges were discussed. We expect that more elaborate and accurate AG propagation measurement campaigns and channel models will be developed in the future, and we hope this study will be of use in that regard.

REFERENCES

- [1] C. S. Sharp, O. Shakernia, and S. S. Sastry, "A vision system for landing an unmanned aerial vehicle," in *Proc. IEEE Int. Conf. Robot. Autom. (ICRA)*, vol. 2. Seoul, South Korea, 2001, pp. 1720–1727.
- [2] G. P. Jones, IV, L. G. Pearlstine, and H. F. Percival, "An assessment of small unmanned aerial vehicles for wildlife research," *Wildlife Soc. Bull.*, vol. 34, no. 3, pp. 750–758, 2006.
- [3] D. H. Shim, H. J. Kim, and S. Sastry, "Control system design for rotorcraft-based unmanned aerial vehicles using time-domain system identification," in *Proc. IEEE Int. Conf. Control Appl.*, Anchorage, AK, USA, 2000, pp. 808–813.
- [4] H. Shim, "Hierarchical flight control system synthesis for rotorcraft-based unmanned aerial vehicles," Ph.D. dissertation, Eng. Mech. Eng., Univ. California at Berkeley, Berkeley, CA, USA, 2000.
- [5] J. D. Blom, *Unmanned Aerial Systems: A Historical Perspective*, vol. 45. Fort Leavenworth, KS, USA: Combat Stud. Inst. Press, 2010.
- [6] M. McFarland, *UPS Drivers May Tag Team Deliveries With Drones*, CNN News, Atlanta, GA, USA, Feb. 2017. [Online]. Available: <https://money.cnn.com/2017/02/21/technology/ups-drone-delivery/index.html>
- [7] J. Desjardins, *Amazon and UPS Are Betting Big on Drone Delivery*, Bus. Insider, New York, NY, USA, Mar. 2018. [Online]. Available: <https://www.businessinsider.com/amazon-and-ups-are-betting-big-on-drone-delivery-2018-3>
- [8] *Amazon Prime Air Drone Delivery*. Accessed: Dec. 10, 2018. [Online]. Available: <https://www.amazon.com/Amazon-Prime-Air/b?ie=UTF8&node=8037720011>
- [9] *Google Project Wing*. Accessed: Dec. 10, 2018. [Online]. Available: <https://x.company/projects/wing/>
- [10] *Google Project Loon*. Accessed: Dec. 10, 2018. [Online]. Available: <https://loon.co/>
- [11] *Uber Elevate*. Accessed: Dec. 10, 2018. [Online]. Available: <https://www.uber.com/us/en/elevate/>
- [12] L. Bandoim, *Uber Plans to Launch Food-Delivery Drones*, Forbes, Jersey City, NJ, USA, Oct. 2018. [Online]. Available: <https://www.forbes.com/sites/lanabandoim/2018/10/23/uber-plans-to-launch-food-delivery-drones/#71c10d17e147>
- [13] J. Johnsson and A. Levin, *Boeing Is Getting Ready to Sell Flying Taxis*, Bloomberg, New York, NY, USA, Mar. 2018. [Online]. Available: <https://www.bloomberg.com/news/articles/2018-03-01/boeing-is-getting-ready-to-sell-flying-taxis-within-a-decade>
- [14] *Zipline Medical Supply Drone Delivery*. Accessed: Dec. 12, 2018. [Online]. Available: <http://www.flyzipline.com/>
- [15] *Flytrex on Demand Drone Delivery*. Accessed: Dec. 12, 2018. [Online]. Available: <http://www.flytrex.com/>
- [16] Wikipedia. *General Atomics MQ-9 Reaper*. Accessed: Jul. 3, 2017. [Online]. Available: https://en.wikipedia.org/wiki/General_Atomics_MQ-9_Reaper
- [17] Goldman Sachs. *Drones: Reporting for Work*. Accessed: Dec. 12, 2018. [Online]. Available: <https://www.goldmansachs.com/insights/technology-driving-innovation/drones/>
- [18] Art Pregler and AT&T. (Feb. 2017). *When COWs Fly: AT&T Sending LTE Signals From Drones*. [Online]. Available: https://about.att.com/innovationblog/cows_fly
- [19] Vodafone. (Nov. 2018). *Beyond Visual Line of Sight Drone Trial Report*. [Online]. Available: https://www.vodafone.com/content/dam/vodafone-images/media/Downloads/Vodafone_BVLOS_drone_trial_report.pdf
- [20] X. Lin *et al.*, "The sky is not the limit: LTE for unmanned aerial vehicles," *IEEE Commun. Mag.*, vol. 56, no. 4, pp. 204–210, Apr. 2018.
- [21] I. Kovacs, R. Amorim, H. C. Nguyen, J. Wigard, and P. Mogensen, "Interference analysis for UAV connectivity over LTE using aerial radio measurements," in *Proc. IEEE Veh. Technol. Conf. (VTC)*, Toronto, ON, Canada, 2017, pp. 1–6.
- [22] R. Amorim, H. Nguyen, P. Mogensen, I. Z. Kovács, J. Wigard, and T. B. Sørensen, "Radio channel modeling for UAV communication over cellular networks," *IEEE Wireless Commun. Lett.*, vol. 6, no. 4, pp. 514–517, Aug. 2017.
- [23] Qualcomm. (May 2017). *LTE Unmanned Aircraft Systems*. [Online]. Available: <https://www.qualcomm.com/media/documents/files/lte-unmanned-aircraft-systems-trial-report.pdf>
- [24] *FAA Small Unmanned Aircraft Regulations*, Federal Aviation Admin., Washington, DC, USA, 2018.
- [25] *Commercial Drone Shipments to Surpass 2.6 Million Units Annually by 2025*, Tractica, Boulder, CO, USA. Accessed: Nov. 28, 2017.
- [26] Qualcomm. *Leading the World to 5G: Evolving Cellular Technologies for Safer Drone Operation*. Accessed: May 17, 2017. [Online]. Available: <https://www.qualcomm.com/invention/technologies/lte/advanced-pro/cellular-drone-communication>
- [27] T. Patterson, *Google, Facebook, SpaceX, OneWeb Plan to Beam Internet Everywhere*. Accessed: May 17, 2017. [Online]. Available: <http://www.cnn.com/2015/10/30/tech/pioneers-google-facebook-spacex-oneweb-satellite-drone-balloon-internet/>

- [28] B. Kerczewski, "Spectrum for UAS control and non-payload communications," in *Proc. IEEE Integr. Commun. Navig. Surveillance Conf. (ICNS)*, 2013, pp. 1–21.
- [29] B. R. Jackson, "Telemetry, command and control of UAS in the national airspace," in *Proc. Eur. Telemetry Test Conf.*, Nuremberg, Germany, 2016, pp. 145–155.
- [30] F. White, "Air-ground communications: History and expectations," *IEEE Trans. Commun.*, vol. 21, no. 5, pp. 398–407, May 1973.
- [31] M. S. B. Mahmoud *et al.*, *Aeronautical Air-Ground Data Link Communications*. New York, NY, USA: Wiley, 2014.
- [32] M. Schnell, U. Epple, D. Shutin, and N. Schneckenburger, "LDACS: Future aeronautical communications for air-traffic management," *IEEE Commun. Mag.*, vol. 52, no. 5, pp. 104–110, May 2014.
- [33] *VHF/UHF Military Monitoring*. Accessed: May 31, 2017. [Online]. Available: http://wiki.radioreference.com/index.php/VHF/UHF_Military_Monitoring
- [34] E. Haas, "Aeronautical channel modeling," *IEEE Trans. Veh. Technol.*, vol. 51, no. 2, pp. 254–264, Mar. 2002.
- [35] B. G. Gates, "Aeronautical communications," *Electr. Eng. III A Radiocommun. J.*, vol. 94, no. 11, pp. 74–81, Mar. 1947.
- [36] D. F. Lamiano, K.-H. Leung, L. C. Monticone, W. J. Wilson, and B. Phillips, "Digital broadband VHF aeronautical communications for air traffic control," in *Proc. Integr. Commun. Navig. Surveillance Conf.*, Arlington, VA, USA, May 2009, pp. 1–12.
- [37] D. W. Matolak, "Air-ground channels & models: Comprehensive review and considerations for unmanned aircraft systems," in *Proc. IEEE Aerosp. Conf.*, Mar. 2012, pp. 1–17.
- [38] C. Levis, J. T. Johnson, and F. L. Teixeira, *Radiowave Propagation: Physics and Applications*. Hoboken, NJ, USA: Wiley, 2010.
- [39] G. M. Djuknic, J. Freidenfelds, and Y. Okuney, "Establishing wireless communications services via high-altitude aeronautical platforms: A concept whose time has come?" *IEEE Commun. Mag.*, vol. 35, no. 9, pp. 128–135, Sep. 1997.
- [40] D. W. Matolak and R. Sun, "Unmanned aircraft systems: Air-ground channel characterization for future applications," *IEEE Veh. Technol. Mag.*, vol. 10, no. 2, pp. 79–85, Jun. 2015.
- [41] A. A. Khuwaja, Y. Chen, N. Zhao, M.-S. Alouini, and P. Dobbins, "A survey of channel modeling for UAV communications," *IEEE Commun. Surveys Tuts.*, vol. 20, no. 4, pp. 2804–2821, 2018.
- [42] M. Asadpour, B. V. den Bergh, D. Giustiniano, K. A. Hummel, S. Pollin, and B. Plattner, "Micro aerial vehicle networks: An experimental analysis of challenges and opportunities," *IEEE Commun. Mag.*, vol. 52, no. 7, pp. 141–149, Jul. 2014.
- [43] Y. Zeng, R. Zhang, and T. J. Lim, "Wireless communications with unmanned aerial vehicles: Opportunities and challenges," *IEEE Commun. Mag.*, vol. 54, no. 5, pp. 36–42, May 2016.
- [44] L. Afonso, N. Souto, P. Sebastiao, M. Ribeiro, T. Tavares, and R. Marinheiro, "Cellular for the skies: Exploiting mobile network infrastructure for low altitude air-to-ground communications," *IEEE Aerosp. Electron. Syst. Mag.*, vol. 31, no. 8, pp. 4–11, Aug. 2016.
- [45] Z. Xiao, P. Xia, and X.-G. Xia, "Enabling UAV cellular with millimeter-wave communication: Potentials and approaches," *IEEE Commun. Mag.*, vol. 54, no. 5, pp. 66–73, May 2016.
- [46] M. Ibrahim and H. Arslan, "Air-ground doppler-delay spread spectrum for dense scattering environments," in *Proc. IEEE Mil. Commun. Conf. (MILCOM)*, Tampa, FL, USA, Oct. 2015, pp. 1661–1666.
- [47] R. Essaadali and A. Kouki, "A new simple unmanned aerial vehicle doppler effect RF reducing technique," in *Proc. IEEE Mil. Commun. Conf.*, Baltimore, MD, USA, Nov. 2016, pp. 1179–1183.
- [48] A. Al-Hourani, S. Kandeepan, and S. Lardner, "Optimal LAP altitude for maximum coverage," *IEEE Wireless Commun. Lett.*, vol. 3, no. 6, pp. 569–572, Dec. 2014.
- [49] X. Cheng, C.-X. Wang, D. I. Laurenson, and A. V. Vasilakos, "Second order statistics of non-isotropic mobile-to-mobile Ricean fading channels," in *Proc. IEEE Int. Conf. Commun. (ICC)*, Dresden, Germany, 2009, pp. 1–5.
- [50] A. Ksendzov, "A geometrical 3D multi-cluster mobile-to-mobile MIMO channel model with Rician correlated fading," in *Proc. IEEE Int. Congr. Ultra Modern Telecommun. (ICUMT) Conf.*, Lisbon, Portugal, 2016, pp. 191–195.
- [51] S. M. Gulfam, S. J. Nawaz, A. Ahmed, and M. N. Patwary, "Analysis on multipath shape factors of air-to-ground radio communication channels," in *Proc. IEEE Wireless Telecommun. Symp. (WTS)*, London, U.K., 2016, pp. 1–5.
- [52] S. M. Gulfam, J. Syed, M. N. Patwary, and M. Abdel-Maguid, "On the spatial characterization of 3-D air-to-ground radio communication channels," in *Proc. IEEE Int. Conf. Commun. (ICC)*, London, U.K., 2015, pp. 2924–2930.
- [53] D. W. Matolak and R. Sun, "Air-ground channel characterization for unmanned aircraft systems: The near-urban environment," in *Proc. IEEE Mil. Commun. Conf. (MILCOM)*, Tampa, FL, USA, 2015, pp. 1656–1660.
- [54] D. W. Matolak and R. Sun, "Air-ground channel characterization for unmanned aircraft systems—Part I: Methods, measurements, and models for over-water settings," *IEEE Trans. Veh. Technol.*, vol. 66, no. 1, pp. 26–44, Jan. 2017.
- [55] S. Kaul *et al.*, "Effect of antenna placement and diversity on vehicular network communications," in *Proc. IEEE Sensor Mesh Ad Hoc Commun. Netw.*, San Diego, CA, USA, Jun. 2007, pp. 112–121.
- [56] A. R. Ruddle, "Simulation of far-field characteristics and measurement techniques for vehicle-mounted antennas," in *Proc. IEE Colloquium Antennas Automotives*, 2000, pp. 1–8.
- [57] W. G. Newhall *et al.*, "Wideband air-to-ground radio channel measurements using an antenna array at 2 GHz for low-altitude operations," in *Proc. IEEE Mil. Commun. Conf. (MILCOM)*, vol. 2. Boston, MA, USA, 2003, pp. 1422–1427.
- [58] D. W. Matolak and R. Sun, "Antenna and frequency diversity in the unmanned aircraft systems bands for the over-sea setting," in *Proc. IEEE Digit. Avionics Syst. Conf. (DASC)*, Oct. 2014, pp. 6A4-1–6A4-10.
- [59] J. Chen, B. Daneshrad, and W. Zhu, "MIMO performance evaluation for airborne wireless communication systems," in *Proc. Mil. Commun. Conf. (MILCOM)*, Baltimore, MD, USA, Nov. 2011, pp. 1827–1832.
- [60] C.-M. Cheng, P.-H. Hsiao, H. T. Kung, and D. Vlah, "Performance measurement of 802.11a wireless links from UAV to ground nodes with various antenna orientations," in *Proc. Int. Conf. Comput. Commun. Netw. (ICCCN)*, Arlington, VA, USA, 2006, pp. 303–308.
- [61] E. Yanmaz, R. Kuschnig, and C. Bettstetter, "Channel measurements over 802.11a-based UAV-to-ground links," in *Proc. IEEE Glob. Commun. Conf. (GLOBECOM) Workshops*, Houston, TX, USA, 2011, pp. 1280–1284.
- [62] T. J. Willink, C. C. Squires, G. W. K. Colman, and M. T. Muccio, "Measurement and characterization of low-altitude air-to-ground MIMO channels," *IEEE Trans. Veh. Technol.*, vol. 65, no. 4, pp. 2637–2648, Apr. 2016.
- [63] D. W. Matolak, H. Jamal, and R. Sun, "Spatial and frequency correlations in two-ray air-ground SIMO channels," in *Proc. IEEE Int. Conf. Commun. (ICC)*, Paris, France, May, 2017, pp. 1–6.
- [64] X. Gao, Z. Chen, and Y. Hu, "Analysis of unmanned aerial vehicle MIMO channel capacity based on aircraft attitude," *WSEAS Trans. Inf. Sci. Appl.*, vol. 10, no. 2, pp. 58–67, 2013.
- [65] C. Zhang and Y. Hui, "Broadband air-to-ground communications with adaptive MIMO datalinks," in *Proc. IEEE Digit. Avionics Syst. Conf. (DASC)*, Seattle, WA, USA, 2011, pp. 4D4-1–4D4-10.
- [66] J. Yang, P. Liu, and H. Mao, "Model and simulation of narrow-band ground-to-air fading channel based on Markov process," in *Proc. Netw. Comput. Inf. Security Conf. (NCIS)*, vol. 1. Guilin, China, 2011, pp. 142–146.
- [67] C. Bluemel, C. Heller, B. Fourestie, and R. Weigel, "Air-to-ground channel characterization for OFDM communication in C-band," in *Proc. Int. Conf. Signal Process. Commun. Syst. (ICSPCS)*, 2013, pp. 1–8.
- [68] M. Simunek, F. P. Fontán, and P. Pechac, "The UAV low elevation propagation channel in urban areas: Statistical analysis and time-series generator," *IEEE Trans. Antennas Propag.*, vol. 61, no. 7, pp. 3850–3858, Jul. 2013.
- [69] V. Vahidi and E. Saberinia, "Orthogonal frequency division multiplexing and channel models for payload communications of unmanned aerial systems," in *Proc. Int. Conf. Unmanned Aircraft Syst. (ICUAS)*, Arlington, VA, USA, 2016, pp. 1156–1161.
- [70] Z. Wu, H. Kumar, and A. Davari, "Performance evaluation of OFDM transmission in UAV wireless communication," in *Proc. Southeastern Symp. Syst. Theory (SSST)*, Tuskegee, AL, USA, 2005, pp. 6–10.
- [71] H. D. Tu and S. Shimamoto, "A proposal of wide-band air-to-ground communication at airports employing 5-GHz band," in *Proc. IEEE Wireless Commun. Netw. Conf. (WCNC)*, Budapest, Hungary, 2009, pp. 1–6.
- [72] W. Khawaja, I. Guvenc, and D. W. Matolak, "UWB channel sounding and modeling for UAV air-to-ground propagation channels," in *Proc. IEEE Glob. Commun. Conf. (GLOBECOM)*, Washington, DC, USA, Dec. 2016, pp. 1–7.

- [73] D. W. Matolak and R. Sun, "Air-ground channel measurements & modeling for UAS," in *Proc. Integr. Commun. Navig. Surveillance Conf. (ICNS)*, 2013, pp. 1–9.
- [74] R. Sun and D. W. Matolak, "Over-harbor channel modeling with directional ground station antennas for the air-ground channel," in *Proc. IEEE Mil. Commun. Conf. (MILCOM)*, Baltimore, MD, USA, 2014, pp. 382–387.
- [75] D. W. Matolak and R. Sun, "Air-ground channel characterization for unmanned aircraft systems: The hilly suburban environment," in *Proc. Veh. Technol. Conf. (VTC)*, Vancouver, BC, Canada, 2014, pp. 1–5.
- [76] R. Sun and D. W. Matolak, "Air-ground channel characterization for unmanned aircraft systems—Part II: Hilly and mountainous settings," *IEEE Trans. Veh. Technol.*, vol. 66, no. 3, pp. 1913–1925, Mar. 2017.
- [77] D. W. Matolak and R. Sun, "Air-ground channels for UAS: Summary of measurements and models for L-and C-bands," in *Proc. Integr. Commun. Navig. Surveillance (ICNS)*, 2016, pp. 8B2-1–8B2-11.
- [78] D. W. Matolak and R. Sun, "Air-ground channel characterization for unmanned aircraft systems—Part III: The suburban and near-urban environments," *IEEE Trans. Veh. Technol.*, vol. 66, no. 8, pp. 6607–6618, Aug. 2017.
- [79] D. W. Matolak, "Channel characterization for unmanned aircraft systems," in *Proc. Eur. Conf. Antennas Propag. (EuCAP)*, Lisbon, Portugal, 2015, pp. 1–5.
- [80] N. Schneckenburger *et al.*, "Measurement of the L-band air-to-ground channel for positioning applications," *IEEE Trans. Aerosp. Electron. Syst.*, vol. 52, no. 5, pp. 2281–2297, Oct. 2016.
- [81] K. Takizawa, T. Kagawa, S. Lin, F. Ono, H. Tsuji, and R. Miura, "C-band aircraft-to-ground (A2G) radio channel measurement for unmanned aircraft systems," in *Proc. Conf. Wireless Pers. Multimedia Commun. (WPMC)*, Sydney, NSW, Australia, 2014, pp. 754–758.
- [82] F. Ono, K. Takizawa, H. Tsuji, and R. Miura, "S-band radio propagation characteristics in urban environment for unmanned aircraft systems," in *Proc. Antennas Propag. (ISAP) Conf.*, Hobart, TAS, Australia, 2015, pp. 1–4.
- [83] N. Goddemeier, K. Daniel, and C. Wietfeld, "Coverage evaluation of wireless networks for unmanned aerial systems," in *Proc. IEEE Glob. Commun. Conf. (GLOBECOM) Workshops*, Miami, FL, USA, 2010, pp. 1760–1765.
- [84] E. Yanmaz, R. Kuschnig, and C. Bettstetter, "Achieving air-ground communications in 802.11 networks with three-dimensional aerial mobility," in *Proc. IEEE INFOCOM*, 2013, pp. 120–124.
- [85] N. Ahmed, S. S. Kanhere, and S. Jha, "On the importance of link characterization for aerial wireless sensor networks," *IEEE Commun. Mag.*, vol. 54, no. 5, pp. 52–57, May 2016.
- [86] E. L. Cid, A. V. Alejos, and M. G. Sanchez, "Signaling through scattered vegetation: Empirical loss modeling for low elevation angle satellite paths obstructed by isolated thin trees," *IEEE Veh. Technol. Mag.*, vol. 11, no. 3, pp. 22–28, Sep. 2016.
- [87] J. Romeu, A. Aguasca, J. Alonso, S. Blanch, and R. R. Martins, "Small UAV radiocommunication channel characterization," in *Proc. Eur. Conf. Antennas Propag. (EuCAP)*, Barcelona, Spain, 2010, pp. 1–5.
- [88] H. T. Kung, C.-K. Lin, T.-H. Lin, S. J. Tarsa, and D. Vlah, "Measuring diversity on a low-altitude UAV in a ground-to-air wireless 802.11 mesh network," in *Proc. IEEE Glob. Commun. Conf. (GLOBECOM) Workshops*, 2010, pp. 1799–1804.
- [89] J. Zelený, F. Pérez-Fontán, and P. Pechac, "Initial results from a measurement campaign for low elevation angle links in different environments," in *Proc. Eur. Conf. Antennas Propag. (EuCAP)*, 2015, pp. 1–4.
- [90] E. Teng, J. Falcao, C. Dominguez, F. Mokaya, P. Zhang, and B. Iannucci, *Aerial Sensing and Characterization of Three-Dimensional RF Fields*, Univ. Buffalo, Buffalo, NY, USA, Sep. 2016.
- [91] Y. S. Meng and Y. H. Lee, "Measurements and characterizations of air-to-ground channel over sea surface at C-band with low airborne altitudes," *IEEE Trans. Veh. Technol.*, vol. 60, no. 4, pp. 1943–1948, May 2011.
- [92] J. Kunisch, I. De La Torre, A. Winkelmann, M. Eube, and T. Fuss, "Wideband time-variant air-to-ground radio channel measurements at 5 GHz," in *Proc. Eur. Conf. Antennas Propag. (EUCAP)*, Rome, Italy, 2011, pp. 1386–1390.
- [93] W. Khawaja, O. Ozdemir, and I. Guvenc, "UAV air-to-ground channel characterization for mmWave systems," in *Proc. IEEE Veh. Technol. Conf. (VTC)*, Toronto, ON, Canada, Sep. 2017, pp. 1–5.
- [94] M. Walter, S. Gligorević, T. Detert, and M. Schnell, "UHF/VHF air-to-air propagation measurements," in *Proc. IEEE Eur. Conf. Antennas Propag. (EuCAP)*, Barcelona, Spain, 2010, pp. 1–5.
- [95] N. Goddemeier and C. Wietfeld, "Investigation of air-to-air channel characteristics and a UAV specific extension to the Rice model," in *Proc. IEEE Glob. Commun. (Globecom) Workshops*, San Diego, CA, USA, Dec. 2015, pp. 1–5.
- [96] Federal Aviation Administration. *FAA Rules for UAVs*. Accessed: Feb. 25, 2017. [Online]. Available: https://www.faa.gov/uas/beyond_the_basics/
- [97] Universitat Politècnica de Catalunya. *Vector Network Analyzer Specifications*. Accessed: May 18, 2017. [Online]. Available: http://www.upc.edu/sct/en/documents_equipament/d_160_id-655-2.pdf
- [98] International Telecommunication Union. *Terrain Cover Types*. Accessed: Jul. 5, 2017. [Online]. Available: <https://www.itu.int/oth/R0A04000031/en>
- [99] International Telecommunication Union. *Propagation by Diffraction*. Accessed: Jul. 5, 2017. [Online]. Available: http://www.itu.int/dms_pubrec/itu-r/rec/p/R-REC-P.526-13-201311-I!!PDF-E.pdf
- [100] M. Kvicerá, F. P. Fontán, J. Israel, and P. Pechac, "A new model for scattering from tree canopies based on physical optics and multiple scattering theory," *IEEE Trans. Antennas Propag.*, vol. 65, no. 4, pp. 1925–1933, Apr. 2017.
- [101] F. Kawamata, "Optimum frame size for land mobile satellite communication channels," in *Proc. IEEE Glob. Commun. (GLOBECOM) Conf.*, vol. 1. Houston, TX, USA, Nov. 1993, pp. 583–587.
- [102] A. A. Aboudebra, K. Tanaka, T. Wakabayashi, S. Yamamoto, and H. Wakana, "Signal fading in land-mobile satellite communication systems: Statistical characteristics of data measured in Japan using ETS-VI," *IEE Proc. Microw. Antennas Propag.*, vol. 146, no. 5, pp. 349–354, Oct. 1999.
- [103] International Telecommunication Union. *Ducting Over Sea Calculation*. Accessed: Jul. 5, 2017. [Online]. Available: http://www.itu.int/md/dologin_md.asp?id=R03-WRC03-C-0025!A27-L188!MSW-E
- [104] Q. Chen, "Wideband channel sounding techniques for dynamic spectrum access networks," Ph.D. dissertation, Elect. Eng. Comput. Sci., Univ. Kansas, Lawrence, KS, USA, 2009.
- [105] J. Parsons, *The Mobile Radio Propagation Channel*, 2nd ed. West Sussex, U.K.: Wiley, 2000.
- [106] J. Chen, D. Raye, W. Khawaja, P. Sinha, and I. Guvenc, "Impact of 3D UWB antenna radiation pattern on air-to-ground drone connectivity," in *Proc. Veh. Technol. Conf. (VTC)*, Chicago, IL, USA, Aug. 2018, pp. 1–5.
- [107] W. Khawaja, O. Ozdemir, F. Erden, I. Guvenc, and D. Matolak, "UWB air-to-ground propagation channel measurements and modeling using UAVs," in *Proc. IEEE Aerosp. Conf.*, 2019.
- [108] W. Khawaja, O. Ozdemir, and I. Guvenc, "Temporal and spatial characteristics of mmWave propagation channels for UAVs," in *Proc. Glob. Symp. Millimeter Waves (GSMM)*, Boulder, CO, USA, May 2018, pp. 1–6.
- [109] A. Paier *et al.*, "Non-WSSUS vehicular channel characterization in highway and urban scenarios at 5.2GHz using the local scattering function," in *Proc. Int. Workshop Smart Antennas*, Vienna, Austria, Feb. 2008, pp. 9–15.
- [110] O. Renaudin, V. M. Kolmonen, P. Vainikainen, and C. Oestges, "Non-stationary narrowband MIMO inter-vehicle channel characterization in the 5-GHz band," *IEEE Trans. Veh. Technol.*, vol. 59, no. 4, pp. 2007–2015, May 2010.
- [111] M. Wentz and M. Stojanovic, "A MIMO radio channel model for low-altitude air-to-ground communication systems," in *Proc. IEEE Veh. Technol. Conf. (VTC)*, Boston, MA, USA, 2015, pp. 1–6.
- [112] A. Al-Hourani, S. Kandepan, and A. Jamalipour, "Modeling air-to-ground path loss for low altitude platforms in urban environments," in *Proc. IEEE Glob. Commun. (GLOBECOM) Conf.*, Austin, TX, USA, 2014, pp. 2898–2904.
- [113] J. Holis and P. Pechac, "Elevation dependent shadowing model for mobile communications via high altitude platforms in built-up areas," *IEEE Trans. Antennas Propag.*, vol. 56, no. 4, pp. 1078–1084, Apr. 2008.
- [114] Q. Feng, J. McGeehan, E. K. Tameh, and A. R. Nix, "Path loss models for air-to-ground radio channels in urban environments," in *Proc. IEEE Veh. Technol. Conf. (VTC)*, vol. 6. Melbourne, VIC, Australia, 2006, pp. 2901–2905.
- [115] N. Schneckenburger, T. Jost, D. Shutin, and U. C. Fiebig, "Line of sight power variation in the air to ground channel," in *Proc. EuCAP*, Davos, Switzerland, 2016, pp. 1–5.
- [116] I. J. Timmins and S. O'Young, "Marine communications channel modeling using the finite-difference time domain method," *IEEE Trans. Veh. Technol.*, vol. 58, no. 6, pp. 2626–2637, Jul. 2009.

- [117] H. Jamal, D. W. Matolak, and R. Sun, "Comparison of L-DACS and FBMC performance in over-water air-ground channels," in *Proc. IEEE Digit. Avionics Syst. Conf. (DASC)*, Prague, Czech Republic, 2015, pp. 2D6-1–2D6-9.
- [118] H. Jamal and D. W. Matolak, "FBMC and L-DACS performance for future air-to-ground communication systems," *IEEE Trans. Veh. Technol.*, vol. 66, no. 6, pp. 5043–5055, Jun. 2017.
- [119] S. Blandino, F. Kaltenberger, and M. Feilen, "Wireless channel simulator testbed for airborne receivers," in *Proc. IEEE Glob. Commun. (GLOBECOM) Workshops*, 2015, pp. 1–6.
- [120] F. Jiang and A. L. Swindlehurst, "Optimization of UAV heading for the ground-to-air uplink," *IEEE J. Sel. Areas Commun.*, vol. 30, no. 5, pp. 993–1005, Jun. 2012.
- [121] M. M. Azari, F. Rosas, K. C. Chen, and S. Pollin, "Optimal UAV positioning for terrestrial-aerial communication in presence of fading," in *Proc. IEEE Glob. Commun. (GLOBECOM) Conf.*, Washington, DC, USA, Dec. 2016, pp. 1–7.
- [122] Z. Yun and M. F. Iskander, "Ray tracing for radio propagation modeling: Principles and applications," *IEEE Access*, vol. 3, pp. 1089–1100, 2015.
- [123] K. Daniel, M. Putzke, B. Dusza, and C. Wietfeld, "Three dimensional channel characterization for low altitude aerial vehicles," in *Proc. Int. Symp. Wireless Commun. Syst. (ISWCS)*, York, U.K., 2010, pp. 756–760.
- [124] Y. Wu *et al.*, "Ray tracing based wireless channel modeling over the sea surface near Diaoyu Islands," in *Proc. Int. Conf. Comput. Intell. Theory Syst. Appl. (CCTSA)*, 2015, pp. 124–128.
- [125] M. Simunek, P. Pechac, and F. P. Fontan, "Excess loss model for low elevation links in urban areas for UAVs," *Radioengineering*, vol. 20, no. 3, pp. 561–568, 2011.
- [126] T. Tavares *et al.*, "Generalized LUI propagation model for UAVs communications using terrestrial cellular networks," in *Proc. IEEE Veh. Technol. Conf. (VTC)*, Boston, MA, USA, 2015, pp. 1–6.
- [127] X. Cai *et al.*, "Low altitude UAV propagation channel modelling," in *Proc. IEEE 11th Eur. Conf. Antennas Propag. (EUCAP)*, Paris, France, 2017, pp. 1443–1447.
- [128] IST-4-027756 WINNER II. (2003). *D1.1.2 V1.0 WINNER II Channel Models*. Accessed: Nov. 29, 2017. [Online]. Available: http://www2.tu-ilmenau.de/nt/generic/paper_pdfs/Part%20II%20of%20D1.1.2.pdf
- [129] T. S. Rappaport, G. R. MacCartney, M. K. Samimi, and S. Sun, "Wideband millimeter-wave propagation measurements and channel models for future wireless communication system design," *IEEE Trans. Commun.*, vol. 63, no. 9, pp. 3029–3056, Sep. 2015.
- [130] T. S. Rappaport. *Investigation of Prediction Accuracy, Sensitivity, and Parameter Stability of Large-Scale Propagation Path Loss Models From 500 MHz to 100 GHz*. Accessed: May 7, 2018. [Online]. Available: http://wireless.engineering.nyu.edu/presentations/NTIA-propagation-presentation-JUNE-15-2016_v1%203.pdf
- [131] T. S. Rappaport, *Wireless Communications: Principles and Practice*, vol. 2. Upper Saddle River, NJ, USA: Prentice-Hall, 1996.
- [132] J. R. Child, "Air-to-ground propagation at 900 MHz," in *Proc. IEEE Veh. Technol. Conf. (VTC)*, vol. 35. Boulder, CO, USA, 1985, pp. 73–80.
- [133] P. J. Park, S.-M. Choi, D. H. Lee, and B.-S. Lee, "Performance of UAV (unmanned aerial vehicle) communication system adapting WiBro with array antenna," in *Proc. Int. Conf. Adv. Commun. Technol. (ICACT)*, vol. 2, 2009, pp. 1233–1237.
- [134] M. Mozaffari, W. Saad, M. Bennis, and M. Debbah, "Mobile unmanned aerial vehicles (UAVs) for energy-efficient Internet of Things communications," *IEEE Trans. Wireless Commun.*, vol. 16, no. 11, pp. 7574–7589, Nov. 2017.
- [135] D. Athukorilage, I. Guvenc, W. Saad, and M. Bennis, "Regret based learning for UAV assisted LTE-U/WiFi public safety networks," in *Proc. IEEE Conf. Glob. Commun. (GLOBECOM)*, Washington, DC, USA, 2016, pp. 1–7.
- [136] M. Alzenad, A. El-Keyi, and H. Yanikomeroglu, "3D placement of an unmanned aerial vehicle base station for maximum coverage of users with different QoS requirements," *IEEE Wireless Commun. Lett.*, to be published.
- [137] E. Kalantari, I. Bor-Yaliniz, A. Yongacoglu, and H. Yanikomeroglu, "User association and bandwidth allocation for terrestrial and aerial base stations with backhaul considerations," in *Proc. Pers. Indoor Mobile Radio Commun. (PIMRC)*, Montreal, QC, Canada, Oct. 2017, pp. 1–6.
- [138] R. I. Bor-Yaliniz, A. El-Keyi, and H. Yanikomeroglu, "Efficient 3-D placement of an aerial base station in next generation cellular networks," in *Proc. IEEE Int. Conf. Commun. (ICC)*, 2016, pp. 1–5.
- [139] M. Alzenad, A. El-Keyi, F. Lagum, and H. Yanikomeroglu, "3D placement of an unmanned aerial vehicle base station (UAV-BS) for energy-efficient maximal coverage," *IEEE Wireless Commun. Lett.*, vol. 6, no. 4, pp. 434–437, Aug. 2017.
- [140] International Telecommunication Union. (2003). *Propagation Data and Prediction Methods Required for the Design of Terrestrial Broadband Millimetric Radio Access Systems*. Accessed: Nov. 27, 2017. [Online]. Available: <http://www.catr.cn/catr/catr/itu/itur/iturlist.jsp?docplace=P&vchar1=P.1410-2>
- [141] R. Sun, D. W. Matolak, and W. Rayess, "Air-ground channel characterization for unmanned aircraft systems—Part IV: Airframe shadowing," *IEEE Trans. Veh. Technol.*, vol. 66, no. 9, pp. 7643–7652, Sep. 2017.
- [142] W. Q. Malik, B. Allen, and D. J. Edwards, "Impact of bandwidth on small-scale fade depth," in *Proc. IEEE Glob. Commun. Conf. (GLOBECOM)*, Washington, DC, USA, Nov. 2007, pp. 3837–3841.
- [143] Y. Zheng, Y. Wang, and F. Meng, "Modeling and simulation of pathloss and fading for air-ground link of HAPs within a network simulator," in *Proc. Int. Conf. Cyber Enabled Distrib. Comput. Knowl. Disc.*, Beijing, China, 2013, pp. 421–426.
- [144] F. Bohagen, P. Orten, and G. E. Oien, "Design of optimal high-rank line-of-sight MIMO channels," *IEEE Trans. Wireless Commun.*, vol. 6, no. 4, pp. 1420–1425, Apr. 2007.
- [145] D. Rieth, C. Heller, D. Blaschke, and G. Ascheid, "On the practicability of airborne MIMO communication," in *Proc. IEEE Digit. Avionics Syst. Conf. (DASC)*, Prague, Czech Republic, 2015, pp. 1–10.
- [146] P. Chandhar, D. Danev, and E. G. Larsson, "Massive MIMO as enabler for communications with drone swarms," in *Proc. Int. Conf. Unmanned Aircraft Syst. (ICUAS)*, Arlington, VA, USA, Jun. 2016, pp. 347–354.
- [147] 3GPP. (2018). *The Mobile Broadband Standard*. [Online]. Available: <http://www.3gpp.org/specifications>
- [148] J. Lyu, Y. Zeng, R. Zhang, and T. J. Lim, "Placement optimization of UAV-mounted mobile base stations," *IEEE Commun. Lett.*, vol. 21, no. 3, pp. 604–607, Mar. 2017.
- [149] V. V. C. Ravi and H. S. Dhillon, "Downlink coverage probability in a finite network of unmanned aerial vehicle (UAV) base stations," in *Proc. IEEE Conf. Signal Process. Adv. Wireless Commun. (SPAWC)*, Edinburgh, U.K., 2016, pp. 1–5.
- [150] "Enhanced LTE support for aerial vehicles specifications, RAN 78." 3GPP, Sophia Antipolis, France, Rep. 36.777. Accessed: May 17, 2018. [Online]. Available: <https://portal.3gpp.org/desktopmodules/Specifications/SpecificationDetails.aspx?specificationId=3231>
- [151] A. Matese *et al.*, "Intercomparison of UAV, aircraft and satellite remote sensing platforms for precision viticulture," *Remote Sens.*, vol. 7, no. 3, pp. 2971–2990, 2015.
- [152] L. Point. *Satellite Versus UAV Mapping: How Are They Different*. Accessed: Nov. 24, 2018. [Online]. Available: <http://www.landpoint.net/satellite-versus-uav-mapping-how-are-they-different/>
- [153] T. C. Tozer and D. Grace, "High-altitude platforms for wireless communications," *Electron. Commun. Eng. J.*, vol. 13, no. 3, pp. 127–137, Jun. 2001.
- [154] "Study on channel model for frequencies from 0.5 to 100 GHz." 3GPP, Sophia Antipolis, France, Rep. ETSI TR 138 901. Accessed: May 17, 2018. [Online]. Available: http://www.etsi.org/deliver/etsi_tr/138900_138999/138901/14.00.00_60/tr_138901v140000p.pdf
- [155] Y. Saleem, M. H. Rehmani, and S. Zeadally, "Integration of cognitive radio technology with unmanned aerial vehicles: Issues, opportunities, and future research challenges," *J. Netw. Comput. Appl.*, vol. 50, pp. 15–31, Apr. 2015.
- [156] P. Jacob, R. P. Sirigina, A. S. Madhukumar, and V. A. Prasad, "Cognitive radio for aeronautical communications: A survey," *IEEE Access*, vol. 4, pp. 3417–3443, 2016.
- [157] G. Stamatescu, D. Popescu, and R. Dobrescu, "Cognitive radio as solution for ground-aerial surveillance through WSN and UAV infrastructure," in *Proc. Conf. IEEE Electron. Comput. Arif. Intell. (ECAI)*, 2014, pp. 51–56.
- [158] T. Wong. *Artificial Intelligence (AI) and Self Driving Cars*. Accessed: May 12, 2018. [Online]. Available: <http://www.semiconwest.org/programs-catalog/smart-automotive-future-smart-connected-self-driving-cars/artificial-intelligence-ai-and-self-driving-cars>
- [159] Tesla. *Full Self Driving Cars*. Accessed: May 12, 2018. [Online]. Available: <https://www.tesla.com/autopilot>
- [160] Radio Technical Commission for Aeronautics. *Command and Control (C2) Data Link Minimum Operational Performance Standards*. Accessed: Jul. 7, 2017. [Online]. Available: https://global.ihs.com/doc_detail.cfm?document_name=RTCA%20DO-362&item_s_key=00694348